Research progress on 2D and 3D mixed-phase perovskite thin films: Fabrication, materials, optimization and characterization

Sustainable Chemistry for Energy Materials 3 (2026) 100028

Contents lists available at ScienceDirect

Sustainable Chemistry for Energy Materials

journal homepage: www.elsevier.com/locate/scenem

Research progress on 2D and 3D mixed-phase perovskite thin films: Fabrication, materials, optimization and characterization

Xiaolan Li [a], Yan Li [a,c,*], Hong He [b], Haoxu Wang [a], Jianhua Chen [a], Xian Gu [a], Zhao Li [a], Jenny Flores Garcia [c], Weiwu Dang [d], Teresa Gatti [c]

[a] School of Materials Science and Engineering, Xi'an Shiyou University, Xi'an 710065, China
[b] Jinduicheng Molybdenum Co., Ltd., Xi'an 710077, China
[c] Politecnico di Torino, Department of Applied Science and Technology, Corso Duca degli Abruzzi 24, Torino 10129, Italy
[d] College of Intelligent Manufacturing, Shaanxi Institute of Technology, Xi'an, Shaanxi 710300, China

ARTICLE INFO

Keywords:
Perovskite solar cell
2D and 3D mixed-phase
2D perovskite
Additive engineering
Oriented growth

ABSTRACT

Three-dimensional (3D) perovskite solar cell (PSC) has emerged as promising candidate for next-generation photovoltaic beyond silicon due to its remarkable power conversion efficiencies (PCE). However, its poor stability remains a major obstacle. Dimensional reduction of 3D perovskite into two-dimensional (2D) structure has proven effective in enhancing stability, leading to growing interest in 2D and 3D mixed-phase PSC that potentially combine durability with high efficiency. Despite these advantages, the incorporation of 2D phases still faces a series of challenges, such as the introduction methods of the 2D phase, the selection of suitable 2D cations, the control of the crystallization behavior in 2D and 3D mixed-phase films, and the development of advanced characterization techniques for identifying and analyzing the 2D phase. Unlike heterojunction structures where 2D perovskite layers are deposited as capping layers atop 3D films, 2D and 3D mixed-phase perovskites incorporate 2D components directly within the 3D matrix, forming localized heterojunctions. In this review, we summarize the fabrication methods for 2D and 3D mixed-phase films, including modified one-step and two-step solution approaches as well as the more recent inverse temperature crystallization (ITC) method. We further discuss the development of novel 2D materials across various perovskite hosts ($CH_3NH_3^+$ (MA^+), $CH(NH_2)_2^+$ (FA^+), Cs^+, multi-cations, and Sn-based systems), although cross-comparisons of identical 2D materials within different host lattices are still lacking. Key optimization strategies, such as additive engineering to improve carrier transport, crystallization control to promote oriented 2D growth, and exploiting the unique nanoplate structures of 2D phases, are highlighted. Finally, we review conventional and advanced characterization techniques that enable structural and stability analysis of 2D and 3D mixed-phase perovskites. This comprehensive overview provides insights into synthesis strategies, targeted material design, performance optimization, and characterization methodologies, thereby guiding the development of high-performance and commercially viable PSCs.

1. Introduction

The remarkable progress of perovskite materials in photovoltaic applications over the past decade has offered promising prospects for the development of high-efficiency and low-cost solar cells. Conventional 3D perovskites adopt the general formula ABX_3, where A represents the smallest monovalent cations, such as MA^+, FA^+, and Cs^+; B is a divalent metal cation (e.g., Pb^{2+} or Sn^{2+}); and X denotes halide anions (e.g., I^-, Br^- and Cl^-). These materials exhibit remarkable characteristics [1], including ultrahigh light absorption coefficients ($>10^5$ cm^{-1}), tunable bandgaps (1.4–2.5 eV), and high charge carrier mobility, which benefits the single-junction PSCs have achieved laboratory efficiencies exceeding 26 % [2,3]. Despite this impressive performance, 3D perovskites suffer from critical limitations: (1) environmental instability, as exposure to moisture, oxygen, light, or heat induces decomposition (e.g., $CH_3NH_3PbI_3$ ($MAPbI_3$) degrades into PbI_2), leading to rapid device degradation; (2) ion migration (e.g., iodine vacancies) causing short operational lifetimes; and (3) stringent encapsulation requirements to

* Correspondence to: School of Materials Science and Engineering, Xi'an Shiyou University, Xi'an, Shaanxi 710065, China.
E-mail address: li1988yan@163.com (Y. Li).

https://doi.org/10.1016/j.scenem.2025.100028
Received 12 October 2025; Received in revised form 14 November 2025; Accepted 26 November 2025
Available online 2 December 2025

block water and oxygen permeation, which increases complexity and cost [3,4].

Fortunately, the distinct atomic configuration within conventional 3D perovskites enables effective compositional engineering at the A, B, and X sites, thereby allowing for precise tuning of material properties. For example, by replacing the smallest monovalent cations at the A-site with large 2D organic cations, 2D perovskites can be obtained. Typical 2D perovskite formulations with the general chemical formula of $A'_mA_{n-1}B_nX_{3n+1}$, where A′ can be a monovalent ($m = 2$) or divalent ($m = 1$) cation that intercalates between the inorganic layers of octahedra and n defines the number of inorganic layers between layers of A′. 2D perovskites with monovalent A′ cations ($m = 2$) form the Ruddlesden-Popper (RP) phase, whereas those with divalent A′ cations ($m = 1$) form the Dion-Jacobson (DJ) phase [4]. In addition to RP and DJ phases, if the guanidinium cations are used at A′ cations, it resides both inside the octahedral cage and in between the layers alternating with another cation, which will form an alternating cation interlayer (ACI) phase [5,6]. 2D perovskites can be regarded as dimensionally reduced versions of their 3D counterparts. As n increases, the bandgap progressively red-shifts, and both the properties and stability gradually approach those of 3D perovskites, Generally, 2D perovskites used in PSCs refer to materials systems with $n \leq 5$ [5].

2D perovskites have attracted significant attention due to their remarkable resistance to external stimuli, the organic part of the 2D perovskite, with the inorganic part inside, forms a layered structure that effectively prevents moisture from penetrating the crystal interior, isolates the stress between crystals, reduces lattice defects, limits the migration of internal ions, and creates a more stable interface within the thin film. This significantly enhances the optical, thermal, and humidity stability of the perovskite film [7]. However, later studies have also confirmed that pure 2D PSCs typically exhibit lower PCEs compared to their 3D counterparts [8]. This performance gap arises from inherent limitations of 2D perovskites: (1) poor charge carrier transport-quantum confinement effects and interlayer energy barriers impede electron and hole mobility, increasing recombination losses; (2) relatively large bandgaps (1.7–2.3 eV), which restrict absorption of low-energy, long--wavelength photons, thereby limiting photocurrent density; and (3) low carrier mobility (1–10 $cm^2/(V{\cdot}s)$), significantly inferior to 3D perovskites (100 $cm^2/(V{\cdot}s)$), hindering efficient charge separation and collection [9]. These drawbacks constrain the practical application of 2D perovskites in high-performance photovoltaics.

Given that 3D perovskite materials exhibit superior optoelectronic properties but suffer from limited stability, while 2D perovskites typically offer enhanced environmental stability at the expense of charge transport and overall device efficiency, the integration of 2D and 3D phases has emerged as a promising strategy to leverage the advantages of both. In 2016, Nazeeruddin et al. [10] (École Polytechnique Fédérale de Lausanne), Mohite et al. [11] (Los Alamos National Laboratory), and Snaith et al. [12] (University of Oxford) independently investigated the fabrication of perovskite films incorporating both 2D and 3D components. Their findings demonstrated that, whether in the form of mixed 2D and 3D phase films or as 2D capping layers forming heterojunctions atop 3D perovskite layers, careful structural engineering can lead to significantly improved device performance. These studies laid a critical foundation for the development of PSCs with both high efficiency and long-term operational stability [13]. The integration of 2D and 3D perovskite phases can be achieved via two main strategies: (1) compositional engineering and (2) interfacial engineering. In the first approach, 2D perovskites or long-chain cations are incorporated directly into the precursor solution of the 3D perovskite. In the second approach, the 2D perovskite precursor or long-chain cations are spin-coated onto a pre-formed 3D perovskite film as a capping layer to form the hybrid structure.

In this review, particular attention is given to 2D and 3D mixed-phase perovskite films, which differ from the heterojunction structures where 2D perovskite layers are deposited as capping layers on top of 3D perovskite films. In 2D and 3D mixed-phase films, as can be seen in Fig. 1, the 2D components are incorporated within the 3D perovskite matrix, forming localized heterojunctions, and the bulk of the 3D material retains its original bandgap, while the phase disorder within the film is significantly reduced [14]. This review will cover the fabrication methods of 2D and 3D mixed-phase films, the key challenges associated with such films and corresponding strategies for addressing them, as well as structural characterization techniques used to analyze the 2D and 3D mixed-phase perovskite films.

2. Fabrication of 2D and 3D mixed-phase perovskite film

2.1. One-step solution method

For 3D perovskites, the one-step solution method typically involves mixing organic and inorganic precursors in a single solution, controlling the film thickness through spin-coating, and subsequently regulating the crystallization behavior of the precursors to finally obtain the perovskite film. For 2D and 3D mixed-phase perovskites, the 2D components are introduced into the 3D perovskite precursor solution, and the amount of incorporated 2D components is precisely controlled to optimize the PCE. For example, to protect $FAMAPbI_3$ perovskite from environmental factors [15], first, the $FAMAPbI_3$ precursor solution was prepared by dissolving CH_3NH_3I (MAI), $CH(NH_2)_2I$ (FAI), and PbI_2 in N, N-Dimethylformamide (DMF) under constant magnetic stirring. Secondly, dodecylammonium chloride (DACl) was introduced in to the as-prepared 3D precursor solution with constant stirring. Thirdly, by adjusting the volume ratio of DACl in $FAMAPbI_3$ at the range to 6 %, the fabricated solar cells exhibited the best PCEs. The crystallization behavior for the 2D and 3D mixed-phase perovskite films via one-step solution process obeys the traditional theory. That is, the rapid solvent evaporation, especially during spin-coating and drying processes, leads to a supersaturated state, which provides the thermodynamic driving force for nucleation. Once the precursor concentration exceeds the solubility limit, nucleation occurs either homogeneously in the bulk or heterogeneously on the substrate. The nucleation density and subsequent crystal growth are determined by the degree of supersaturation resulting from the dynamics of solvent removal. By controlling the supersaturation and optimizing the annealing conditions, uniform crystal growth can be achieved, resulting in compact and highly crystalline perovskite films, which are essential for efficient device performance [16].

Many studies have also shown that 2D perovskite tends to precipitate at the surface and interface of 3D films, forming a discontinuous aggregated localized heterojunction in the film. It can be speculated that the localized 2D and 3D heterojunctions are random and lack order. To improve the controllability of 2D perovskite distribution within the 3D matrix, Sun et al. [17] attempted to dissolve dimethylammonium iodide (DMAI) in isopropanol (IPA) to form a low concentration 2D component. After obtaining the 3D perovskite film, the DMAI solution was spin-coated onto the 3D film to form a disconnect passivated state. Comparably, Zou et al. [18] deposited the $MAPbI_3$ perovskite with residual PbI_2, and without decreasing the concentration the n-butylammonium iodide (BAI), a 2D perovskite layer is formed on the surface of $MAPbI_3$ perovskite via the chemical reaction between BAI and residual PbI_2. To enhance the mixing between the 2D and 3D phases, Li et al. [19] employed a bottom-up passivation strategy, as shown in Fig. 2a. In their approach, a highly concentrated phenethylammonium bromide (PEABr) solution was first spin-coated onto the substrate, followed by spin-coating the 3D perovskite precursor solution on top. By taking advantage of the solubility of PEABr salts in the subsequently deposited 3D perovskite solvent, they were able to regulate the diffusion behavior of PEABr within the 3D precursor solution. Combined with the rapid crystallization induced by the antisolvent method, an improved mixed state between 2D and 3D perovskite was achieved. The conventional precursor-mixing method, which prepares materials by dissolving

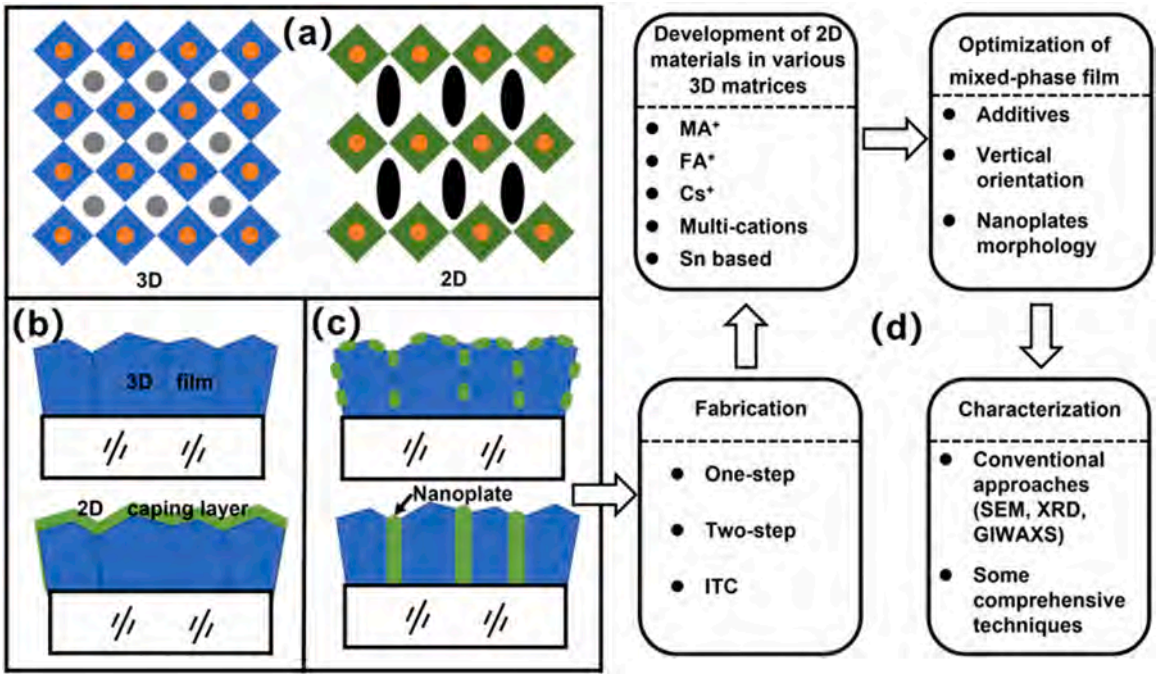

Fig. 1. Comparison of the crystal structures of 3D and 2D perovskites (a); schematic illustration of 3D perovskite and 2D perovskite used as a capping layer on top of a 3D perovskite film (b); schematic diagram showing the formation of 2D and 3D mixed-phase films via 2D perovskite precipitating at the surface/interface of 3D perovskites, as well as being distributed within the 3D perovskite film in the form of nanoplates (c); and the main topics of this review, including the fabrication of 2D and 3D mixed-phase perovskite films, the development of 2D materials, the structural optimization of 2D and 3D mixed-phase films, and their characterization (d).

them according to the desired stoichiometric ratios, is prone to stoichiometric deviations due to the presence of impurities or non-perovskite phases. Therefore, a precrystallization strategy is tried [20], a mixed solution of 2D $(3\text{-TMA})_2PbCl_4$ (3-TMA refers to 3-thiophenemethylammonium) and 3D component is first crystallized into a solid powder with high crystallinity, high purity, and precise stoichiometry. The resulting powder is then dissolved and deposited into perovskite films by one-step solution method.

2.2. Two-step solution method

In contrast to the aforementioned one-step solution method, in the two-step method, separate solutions of the organic and inorganic precursors are first prepared. The inorganic precursor is deposited to form a film, which then reacts with the organic precursor through a subsequent contact reaction to yield the perovskite film. Zhou et al. [23] aimed to incorporate 3-thiophenemethylammonium (ThMA) cations into an MAFA 3D perovskite. First, they prepared a PbI_2 precursor solution to deposit a PbI_2 film. Then, a solution of FAI: MAI: MACl with varying ThMAI content was spin-coated on top of the PbI_2 layer, followed by thermal annealing, resulting in a 2D and 3D mixed-phase perovskite. Zhang et al. [21] designed and synthesized a π-conjugated organic spacer molecule (*Z*)-2-([1,1′-biphenyl]-4-yl)-3-(5-(4-(3-aminopropoxy) phenyl) thiophen-2-yl)acrylonitrile (abbreviated as BPCSA-S). As shown in Fig. 2b, BPCSA-S·hydroiodic acid (HI) and PbI_2 powder were fully dissolved to prepare an inorganic precursor solution, which was then spin-coated to form a film. Subsequently, a mixed solution of FAI, MACl, and MAI was deposited onto the PbI_2 film and annealed, resulting in a 2D and 3D mixed-phase perovskite film. By virtue of the cyano, thiophene, and amino functional groups in BPCSA-S, the molecule can trigger the in-situ growth of 2D perovskites, which subsequently serve as a template to promote the heteroepitaxial growth of 3D perovskites, thereby yielding a high-quality, low-defect 2D and 3D mixed-phase perovskite film.

In order to investigate the formation mechanisms of these mixed-dimensional perovskite phases, Xiang et al. [24] investigated the evolution of mixed-dimensional perovskite phases in one-step and two-step fabrication processes by introducing hexadecyltrimethylammonium bromide (HTAB) ligand molecules into the perovskite precursor solution. They found that, in the two-step process, the 2D perovskite phases evolved sequentially from 2D-α/β/γ (formed with the assistance of IPA solvent) → 2D-7.6° (induced by thermal annealing) → 2D-7.3° (formed upon further annealing). In contrast, the one-step process exhibited a distinct evolution pathway, that is 2D-7.6° (generated through the reaction between HTAB ligands and the intermediate phases) → 2D-7.3°. Specifically, the 2D-α/β/γ phases formed ultrathin belt-like crystals covering the surface of the 3D perovskite; the 2D-7.6° phase tended to encapsulate the 3D perovskite grains without showing clear crystal morphology; and the 2D-7.3° phase developed as platelet-shaped crystals dispersed among the 3D grains. As a result, the PCE of PSCs fabricated via the two-step sequential deposition method increased from 23.22 % to 24.54 %, whereas the PCE of devices prepared using the one-step nitrogen-blowing method improved from 20.3 % to 21.13 %. Based on these outcomes, the two-step solution process yields superior device performance. However, despite the enhanced photovoltaic performance of films produced via the two-step approach, this method still shares a common drawback with other two-step solution processes, namely the presence of residual unreacted PbI_2 [25].

2.3. ITC method

The ITC method was first reported by Huang et al. [26] for the growth of multi-cations perovskite single crystals. By employing HI as an additive and utilizing the principle that the solubility of the precursor decreases with increasing temperature, they successfully designed a series of multi-cations perovskite single crystals. Single-crystal characterization revealed that the incorporation of 15 % MA^+ into $FAPbI_3$ stabilized a phase with superior charge transport properties, and the $FA_{0.85}MA_{0.15}PbI_3$ single crystal exhibited suppressed ion migration. In order to mitigate defects and degradation pathways associated with excessive grain boundaries in polycrystalline films, as shown in Fig. 2c

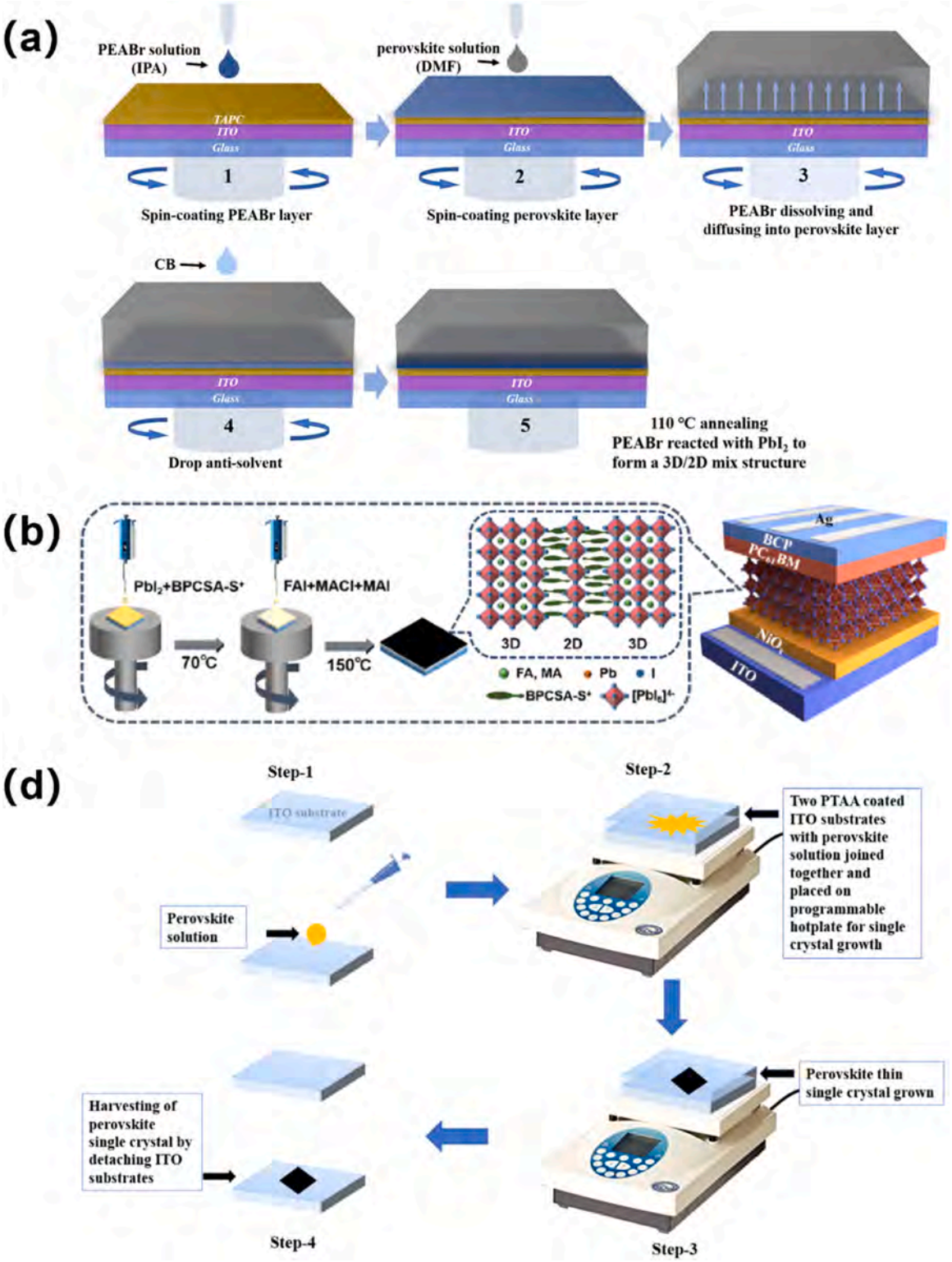

Fig. 2. Schematic illustration of three common methods for preparing 2D and 3D mixed-phase perovskite films: (a) one-step solution method [19], (b) two-step solution method [21], and (c) ITC method [22]. For ITC process, a 2D/3D mixed precursor solution was first prepared and injected into a cavity on a substrate preheated to 70 °C, with a spacing of 25 μm, in order to control the thickness of the perovskite film. The temperature was then gradually increased from 70 °C to 110 °C at a rate of 5 °C per hour, allowing crystallization to occur due to the decreased solubility of the precursor at elevated temperatures, thereby producing 2D and 3D mixed-phase perovskite films. Permission to use the figures has been obtained from the American Chemical Society, Elsevier and John Wiley and Sons, and the corresponding Copyright Clearance Centers.

Younas et al. [22] prepared two types of 2D and 3D mixed precursor solutions (BAI: $MAPbI_3$ and Phenylammonium iodide (PAI) : $MAPbI_3$) and injected them into 25 μm-spaced cavities on a substrate preheated to 70°C, preventing excessive film thickening during growth. The temperature was then gradually increased from 70°C to 110°C at a rate of 5°C per hour, enabling crystallization via the reduced solubility of precursors at elevated temperatures, ultimately yielding 2D and 3D mixed-phase perovskite films. Inspired by the ITC strategy, Chen et al. [27] synthesized $iBA_2MA_{n-1}Pb_nI_{3n+1}$ 2D and 3D mixed-phase single crystals, where iBA refers to iso-Butylammonium, which were subsequently redissolved and processed into perovskite films using a one-step solution method. The authors highlighted that when these hybrid crystals were redissolved, the crystallization process essentially involved a reassembly of the components, and the long-chain iBA molecules remained at the grain boundaries and surfaces of the films.

3. Development of 2D materials for 2D and 3D mixed-phase perovskite film

Currently, there are many types of 2D materials, and some empirical guidelines have been established for their selection. Zou et al. [28] investigated the transformation of 3D phase into 2D phases induced by using large organic cations, noting that different cations exhibit distinct tendencies toward interfacial modification and bulk passivation, and that aromatic spacers, with their π-conjugated structures and higher dielectric constants, generally improved charge transportation compared to aliphatic spacers. Li et al. [29] further demonstrated that the n-value in 2D perovskites critically influences device performance; 4-Aminoethylpyridine (4-AEP) cations induce low-n 2D phases at 3D grain boundaries, whereas PEA generates high-n quasi-2D phases, with 4-AEP-doped $MAPbI_3$ PSCs achieving higher PCE of 20.7 % than PEA-based quasi 2D and 3D devices. Jiang et al. [30] emphasized that the conventional view of octylammonium sulfate (OAS) passivation, coordination with unpaired Pb^{2+} or halide ions, often neglects interactions with excess PbI_2. Their work showed that OASs not only directly passivate defects but also redistribute aggregated PbI_2 into discontinuous layers, enhancing overall passivation. Recently, double perovskites have emerged as promising candidates for 2D component due to their low toxicity and high stability, potentially joining the pool of strategies for stabilizing perovskites. Collectively, there is a wide variety of 2D materials, and the underlying principles and mechanisms for their proper and rational utilization still require further investigation. In the following, we classify and review recent advances in 2D materials according to their functional roles in series perovskite films matrix [31], as shown in Table 1, they were divided into the group of MA^+, FA^+, Cs^+, Multi-cations, and Sn-based.

3.1. MA^+ cations perovskite

MA^+ has been extensively investigated due to its outstanding optoelectronic properties. However, MA^+ perovskites are extremely sensitive to moisture, where water can trigger hydrolysis reactions, leading to phase degradation. Under illumination, the migration of MA^+ and halide ions further aggravate ion redistribution, causing defect accumulation at grain boundaries and phase segregation [32]. To address these issues, numerous studies have introduced large 2D component into the perovskite composition. Li et al. [33] developed a 4, 4′-bipiperidine (BiPi) organic salt with excellent stability and successfully incorporated it into perovskites. The embedded BiPi organic salt improved the crystallinity of the perovskite material, promoted the formation of mixed 2D and 3D perovskite phases, and passivated defects within the perovskite layer, thereby prolonging carrier lifetimes. As a result, the optimized PSCs achieved a PCE of 20.03 %, with an open-circuit voltage (V_{oc}) of 1.10 V, a short-circuit current density (J_{sc}) of 23.5 mA cm^{-2}, and a fill factor

Table 1
2D components employed in recent studies on 2D and 3D mixed perovskite films, device architectures based on 2D and 3D mixed-phase film assembly, and the corresponding optimal photovoltaic performance.

	Organic cation or components of 2D perovskite	Device structure	V_{oc} / V	J_{sc} / mA·cm^{-2}	FF / %	PCE / %	ref
MA^+	$BiPiI_2$	FTO/TiO_2/mixed phase perovskite/Spiro-OMeTAD/Au	1.10	23.51	77.00	20.03	32
	$C_mH_{2m+1}NH_3^+Cl^-$(m=8/10/12)	FTO/TiO_2/mixed phase perovskite /Spiro-OMeTAD/Au	0.94	17.00	50.00	8.00	33
	$HOOC(CH_2)_4NH_3I$, AVAI	FTO/c-TiO_2/mp-TiO_2/mixed phase perovskite/Spiro-OMeTAD/Au	1.025	18.84	75.50	14.60	10
	BA_2PbI_4	FTO/TiO_2/PCBM/mixed phase perovskite /Spiro-OMeTAD/Au	1.17	23.04	57.09	15.39	36
	DAI	ITO/TiO_x/mixed phase perovskite /Spiro-OMeTAD/MoO_3/Ag	1.05	22.95	79.04	19.05	35
	$(PBA_{0.5}BA_{0.5})_2MA_3Pb_4I_{13}$	ITO/PTAA/mixed phase perovskite /PCBM/BCP/Ag	1.19	17.30	78.00	16.00	34
FA^+	$(4AP)PbI_4$	FTO/TiO_2/mixed phase perovskite /Spiro-OMeTAD/Au	1.18	25.70	81.81	24.90	40
	PEA_2PbI_4	ITO/SnO_2/mixed phase perovskite /Spiro-OMeTAD/Au	1.13	24.44	76.50	21.06	42
	PEA/NEA/PyBA	ITO/SnO_2/mixed phase perovskite /Spiro-OMeTAD/Au	1.18	25.80	83.00	25.30	43
	4-F-PEAI	ITO/SnO_2/mixed phase perovskite /Spiro-OMeTAD/Ag	1.11	24.81	78.40	21.60	41
Cs^+	$EDAPbI_4$	ITO/SnO_2/c-TiO_2/mixed phase perovskite/Spiro-OMeTAD/Ag	1.15	14.53	71.00	11.86	45
	Gly-X: X = Cl, Br, and I	FTO/TiO_2/mixed phase perovskite/Spiro-OMeTAD/Au	1.33	16.04	80.92	17.26	47
	$Cs_2PbI_2Cl_2$	FTO/ compact-TiO_2/ mixed phase perovskite/Spiro-OMeTAD/Au	1.21	16.62	75.17	15.09	46
Multi-cations	$(NpMA)_2PbI_4$	ITO/SnO_2/mixed phase perovskite/Spiro-OMeTAD/Ag	1.18	24.97	81.36	24.37	51
	AVAI/GAI/β-GUA	ITO/SnO_2/ZnO/mixed phase perovskite/Spiro-OMeTAD/Ag	1.14	24.41	79.6	22.20	50
	ThMA	ITO/SnO_2/mixed phase perovskite/Spiro-OMeTAD/MoO_3/Ag	1.16	22.88	81.00	21.49	21
	PMAI/PEAI/PPAI/PBAI	ITO/PTAA/Al_2O_3/ mixed phase perovskite/C60/SnO_2/Ag	1.08	25.56	81.90	22.68	52
	TAPPyI	FTO/TiO_2/mixed phase perovskite/Spiro-OMeTAD/Au	1.19	24.63	77.30	22.73	53
	CEA^+ and BEA^+	FTO)/cTiO_2/m-TiO_2/ mixed phase perovskite/Spiro-OMeTAD/Au	1.1	22.77	79.91	20.08	54
	ODA^+	ITO/PTAA/ mixed phase perovskite /PC61BM/BCP/Ag	1.26	21.60	81.60	22.19	55
	PhFACl	ITO/SnO_2/mixed phase perovskite/Spiro-OMeTAD/MoO_3/Ag	1.16	24.67	81.54	23.36	56
	$(PA)_2PbI_4$	FTO/cTiO_2/m-TiO2/ mixed phase perovskite/Spiro-OMeTAD/Au	1.06	21.90	74.38	17.23	31
	BA	FTO/SnO_2/$PC_{61}BM$/mixed phase perovskite/spiro-OMeTAD/Au	1.14	22.70	80.00	20.60	12
	DACl	ITO/PEDOT:PSS/mixed phase perovskite/spiro-OMeTAD/Ag	0.85	13.57	44.00	5.00	15
	PEA_2PbI_4	FTO/TiO_2/mixed phase perovskite/Spiro-OMeTAD/Au	1.22	23.36	73.00	20.80	49
Sn-based	$EDAI_2$ and PEAI	ITO/PEDOT:PSS/mixed phase perovskite/PCBM/BCP/Ag	0.63	19.32	69.43	8.47	59
	FPEABr	ITO/PEDOT:PSS/mixed phase perovskite/ICBA/BCP/Al	0.84	24.91	70.76	14.81	57
	PEAI	ITO/PEDOT:PSS/mixed phase perovskite/ICBA/BCP/Ag	0.73	22.79	66.00	11.03	58

(FF) of 0.77, which represents a 13 % improvement compared with the pristine devices. Holanda et al. [34] deposited chloride solutions of alkylammonium salts containing 8, 10, and 12 carbon atoms (octyl-, decyl-, and dodecylammonium chloride, respectively) on the surface of 3D perovskite films, thereby synthesizing a series of 2D and 3D mixed-phase perovskite films in situ. They found that as the alkyl chain length increased (C8 > C10 > C12), the environmental stability of the 2D and 3D mixed-phase films decreased. Chen et al. [35] synthesized an aliphatic RP perovskite film, $(PBA_{1-x}BA_x)_2MA_3Pb_4I_{13}$ (BA refers to n-butylammonium, and PBA refers to 4-phenylbutylammonium). The resulting film exhibited an increased colloidal particle size, reduced nucleation sites, and extremely smooth films with significantly lower trap densities, thereby enhancing electron transport. In addition, continuous research in recent years has reported that Bis (4-aminobutylammonium) lead(II) tetraiodide [10], diethylammonium iodide (DAI) [36], BA_2PbI_4 [37], and 2D alkylammonium halide perovskites [38] also contribute to defect passivation in MA^+ perovskite films. Unfortunately, despite the enhanced stability achieved through dimensional reduction, the highest efficiencies of these reported devices still fall behind of the record efficiencies attained by pure-phase MA^+ PSCs.

3.2. FA^+ cations perovskite

FA^+ perovskite is considered an ideal material for single-junction solar cells owing to its favorable optoelectronic properties, such as a high absorption coefficient, long carrier diffusion length, and an optimal bandgap of 1.48 eV [39]. However, its phase instability remains one of the major obstacles hindering commercial applications. Specifically, the black photoactive phase (α-phase or γ-phase, with cubic or trigonal crystal structures) tends to spontaneously transform at room temperature into the yellow non-perovskite δ-phase (hexagonal structure), which exhibits negligible photovoltaic activity. In addition, during crystallization, a so-called "volume collapse" often occurs, leading to the formation of numerous voids and bulk defects within the film and at the grain boundaries [40]. These defects not only serve as non-radiative recombination centers, thereby reducing device efficiency, but also provide pathways for ion migration as well as moisture and oxygen infiltration, which greatly accelerate phase decomposition and device degradation.

Yang et al. [41] found that the relatively large FA^+ cation induces distortions in the octahedral framework. When reassembled with smaller ammonium ligands (e.g. BA^+) into 2D perovskites, these distortions aggravate interfacial defects, making it difficult to obtain highly stable 2D and 3D mixed-phase perovskite. In contrast, compared with conventional simple ammonium ligands, amidine-based ligands possess more suitable molecular sizes and richer N-H groups, which enable the formation of multiple hydrogen bonds with octahedra. This significantly reduces interfacial defects and greatly enhances the intrinsic stability of the material. Based on molecular structure comparison, they selected 4-aminopyridine (4AP) as 2D component. They compared the crystallization processes of pure 3D perovskites and 2D and 3D mixed-phase perovskites (Fig. 3a). For the 3D case, during spin-coating, FA-rich α-phase perovskite preferentially formed, and upon thermal annealing, the removal of residual DMSO from the bulk induced dissolution-recrystallization processes. Under this equilibrium and solvent evaporation, homogeneous nucleation occurred, eventually leading to structural collapse of the 3D perovskite and void formation at grain boundaries. In sharp contrast, the 4AP cations guided the formation of DJ-type 2D perovskites in the 3D matrix, which acted as a structural framework to support the growth of the 3D α-phase perovskite. This altered the nucleation/growth pathway, prevented volume collapse, and, due to the buffering effect of the 2D component, relieved lattice-mismatch-induced stress. As a result, the 3D $FAPbI_3$ lattice exhibited higher stability during thermal cycling, thereby enhancing phase stability of α-$FAPbI_3$.

Wang et al. [42] proposed a synergistic strategy combining co-regulation and co-passivation to stabilize $FAPbI_3$. Specifically, they introduced 4-fluorophenylethylammonium iodide (4-F-PEAI) into the precursor solution and polyvinylcarbazole (PVK) into the antisolvent. The N and F atoms in both 4-F-PEAI and PVK possess lone-pair electrons, which acted as Lewis bases to coordinate with Pb^{2+} in the precursor. This temporary coordination effectively "locked" Pb^{2+} ions, reducing the crystallization driving force, slowing down nucleation and crystal growth, and allowing sufficient time for ordered atomic/ionic arrangement. Transmission electron microscopy (TEM) analyses were conducted on the as-prepared 2D and 3D mixed-phase perovskite film, revealing two characteristic regions: region I (grain interiors) and region II (grain boundaries) (Fig. 3b). They found the high-resolution TEM and fast Fourier transform (FFT) images of region I showed a lattice spacing of 3.18 Å (Fig. 3c), consistent with the (002) plane of cubic $FAPbI_3$. In contrast, region II exhibited a larger spacing of 7.13 Å (Fig. 3d), matching the (002) plane of $FPEA_2PbI_4$, confirming the formation of 2D perovskite at grain boundaries. To further elucidate the cooperative effect of 4-F-PEAI and PVK during $FAPbI_3$ crystallization, they performed scanning electron microscopy (SEM) analyses on pristine 3D, 3D treated with 4-F-PEAI (3D-2D), 3D treated with both 4-F-PEAI and PVK (3D-2D-PVK) samples (Fig. 3e-g). They found all three exhibited dense grain packing without pinholes, minimizing leakage pathways. They also found that PVK residues remained on the surface of the 3D-2D-PVK films (Fig. 3g), forming fragmented island-like structures. These ultrathin 2D layers at grain boundaries effectively encapsulated the exposed 3D grains, directly passivating dangling bonds and uncoordinated ions. Ultimately, in their investigation, owing to the synergistic effects of grain-boundary engineering and crystallization kinetics regulation, the crystallization quality, defect density, ion migration barriers, and environmental stability of $FAPbI_3$ films were fundamentally improved, thereby achieving superior phase stability of α-$FAPbI_3$. Lee et al. [43] achieved phase stabilization of $FAPbI_3$ by incorporating the 2D component phenylethylammonium (PEA) into the $FAPbI_3$ precursor solution. In addition to PEA, Zhang *et al.* [44] introduced highly conjugated organic spacers, naphthylethylamine (NEA), and pyrenebutanamine (PyBA), as 2D component for phase stabilization of $FAPbI_3$, and their study revealed that the highly conjugated PyBA spacer was the most effective moisture barrier to protect the 3D perovskite phase.

3.3. Cs^+ cations perovskite

Both MA^+ and FA^+ are organic cations whose internal chemical bonds (e.g., C-N, N-H, and C-H) are relatively weak compared to inorganic ions. Under thermal stress, light irradiation, or humid environments, they are prone to decomposition or volatilization. Once A-site cations are lost, the ABX_3 perovskite crystal structure collapses, leading to a complete loss of optoelectronic functionality. In contrast, in $CsPbX_3$, Cs^+ ions are strongly bonded to the surrounding octahedral framework through ionic interactions, rendering the structure robust, less volatile, and resistant to decomposition. However, due to the small tolerance factor, Cs^+ cannot stably sustain the PbI_6 framework at room temperature. As a result, α-$CsPbI_3$ spontaneously transforms into the non-perovskite δ-$CsPbI_3$ phase at ambient conditions, thereby losing its photoactive properties. This presents a dilemma for researchers, as $CsPbI_3$ exhibits high thermal stability but poor phase stability of δ-$CsPbI_3$ at room temperature.

Based on first-principles calculations using the stochastic surface walking method [45], revealed the multi-step phase transition kinetics of $CsPbI_3$ from the photoactive γ to δ phase at the atomic scale, as illustrated in Fig. 4a. The transition does not occur in a single step but instead proceeds through three intermediate states (MS1, MS2, and MS3). The pathway involves the "breaking of corner-sharing octahedral connections" and the "formation of edge-sharing octahedral connections." Among these steps, the γ → MS1 transition was identified as the rate-determining step. The overall energy barrier for the transformation

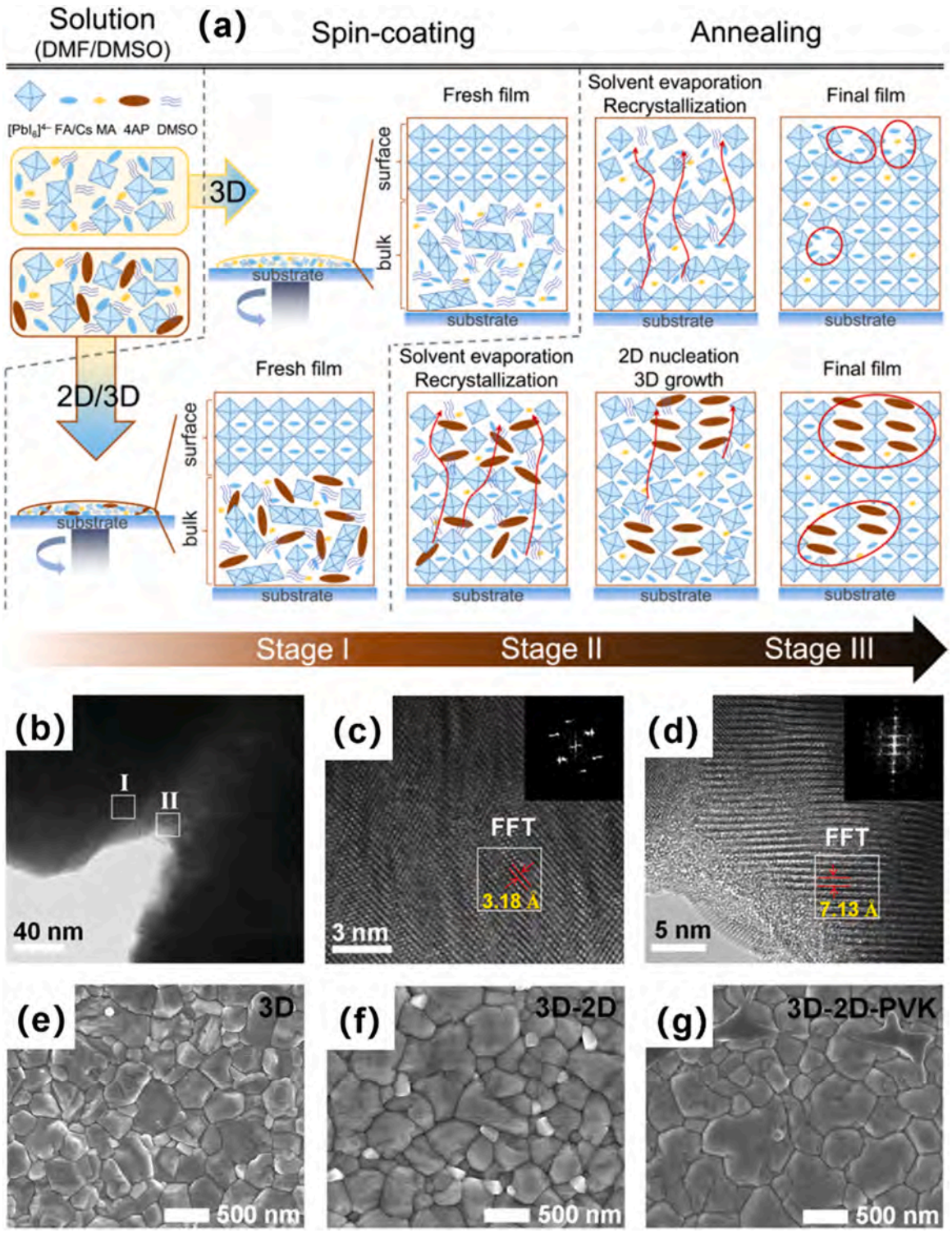

Fig. 3. A comparative schematic illustrates the crystallization processes of pure 3D perovskites film and 2D and 3D mixed-phase perovskite film (a) [41]: the 4AP cations guided the formation of DJ-type 2D perovskites in the 3D matrix, which acted as a structural framework to support the growth of the 3D α-phase perovskite, and this altered the nucleation/growth pathway, prevented volume collapse. the TEM and FFT results(b-d), and the SEM results (e-g) of the as-prepared 2D and 3D mixed-phase perovskite film [42]. Permission to use the figures has been obtained from the Elsevier and John Wiley and Sons, and the corresponding Copyright Clearance Centers.

from the 3D corner-sharing octahedral network to the 2D layered structure and subsequently to the one-dimensional edge-sharing octahedral chains was found to be only ~30 meV/atom, which is significantly lower than the previously assumed one-step barrier (~103 meV/atom). The presence of intermediate states markedly reduces the phase transition barrier, and employing 2D perovskites has been proven to be an efficient strategy for stabilizing $CsPbI_3$.

Zhang *et al.* [46] introduced ethylenediammonium lead iodide ($EDAPbI_4$) as a stabilizer. The EDA cation contains two positively charged amino groups ($-NH_3^+$), which can act like "hands" that grasp

neighboring $CsPbI_3$ grains, forming a 3D crosslinked network through strong ionic and hydrogen bonds that bind the $CsPbI_3$ grains together. In addition, $EDAPbI_4$ crystals grow along the (110) orientation, which can form coherent or semi-coherent interfaces with the $CsPbI_3$ lattice. This configuration reduces lattice mismatch and interfacial stress, thereby firmly "locking" the $CsPbI_3$ grains in place and suppressing phase transition. With this combined (110)-oriented layered structure and crosslinking design, experimental results demonstrated that the α-to-δ phase transition of $CsPbI_3$ was effectively inhibited, achieving long-term stability at both room temperature and 100°C, while also improving the optoelectronic performance. However, X-ray diffraction (XRD) analysis of $CsPbI_3$·x$EDAPbI_4$ samples (Fig. 4b) revealed that no characteristic diffraction peaks corresponding to the $EDAPbI_4$ phase ($2\theta < 10°$) were observed. This indicates that XRD alone may not be sufficient to confirm the presence of 2D and 3D mixed-phase. Owing to its excellent thermal stability, all-inorganic $Cs_2PbI_2Cl_2$ [47] was also selected as a stabilizer. According to high-resolution transmission electron microscopy (HRTEM) analysis (Fig. 4c-g), $Cs_2PbI_2Cl_2$ was found to anchor onto $CsPbI_{2.5}Br_{0.5}$. The (003) plane spacing of $Cs_2PbI_2Cl_2$ was measured to be 6.16 Å, while the (001) plane spacing of $CsPbI_{2.5}Br_{0.5}$ was 6.06 Å, corresponding to a lattice mismatch of only 1.6 %. Therefore, the two lattices can form a continuous and smooth transition without generating significant defects or dangling bonds, resulting in a well-connected interface that effectively reduces the interfacial energy. Xu et al. [48] designed and synthesized three glycine halides (Gly-X, X = Cl, Br, I) as 2D agents, and density functional theory (DFT) calculations directly showed that after Gly-I treatment, the activation energy for iodine vacancy migration increased by more than sixfold. TEM and FFT diffraction patterns revealed that the region between two 3D grains exhibited a 2D Gly_2PbI_4 crystal structure, and this confirmed that the 2D structure precisely encapsulated the 3D grains, physically blocking the phase transition pathways.

3.4. Multi-cations perovskite

Multi-cations perovskite (e.g., Cs/FA/MA systems) has demonstrated enhanced device efficiency and stability through the synergistic effect of multiple A-site cations; however, compositional segregation remains a key degradation mechanism. For example, in $FA_{1-x}Cs_xPbI_3$ perovskite films, under stimuli, Cs^+ (ionic radius ≈ 1.81 Å) migrates toward the surface, forming a ~10 nm Cs-rich layer, while FA^+ (ionic radius ≈ 2.53 Å) accumulates at the bottom. This compositional gradient broadens the bandgap at the surface and narrows it at the bottom, resulting in carrier transport barriers. More critically, Cs-rich clusters exhibit accelerated photoluminescence (PL) decay under illumination [49]. Because vertically oriented 2D layers, aligned perpendicular to the substrate, can effectively block the longitudinal migration channels of A-site cation (e.g., Cs^+ and FA^+), thereby incorporation of 2D perovskites to suppress such ion migration pathways may be useful.

To date, a series of novel 2D perovskite materials have been successfully applied in multi-cations perovskite systems. Zhai et al. [50] use a mixed solution of MAI and phenylethylammonium iodide (PEAI) to react with intentionally excess PbI_2 in Cs/MA/FA multi-cations perovskite layers. They formed $MAPbI_3$/(Cs/MA/FA) heterostructures and 2D PEA_2PbI_4 passivation layers, and the PSCs show an increased V_{oc}, J_{sc}, and FF. Yao et al. [51] introduced β-guanidinopropionic acid (β-GUA)

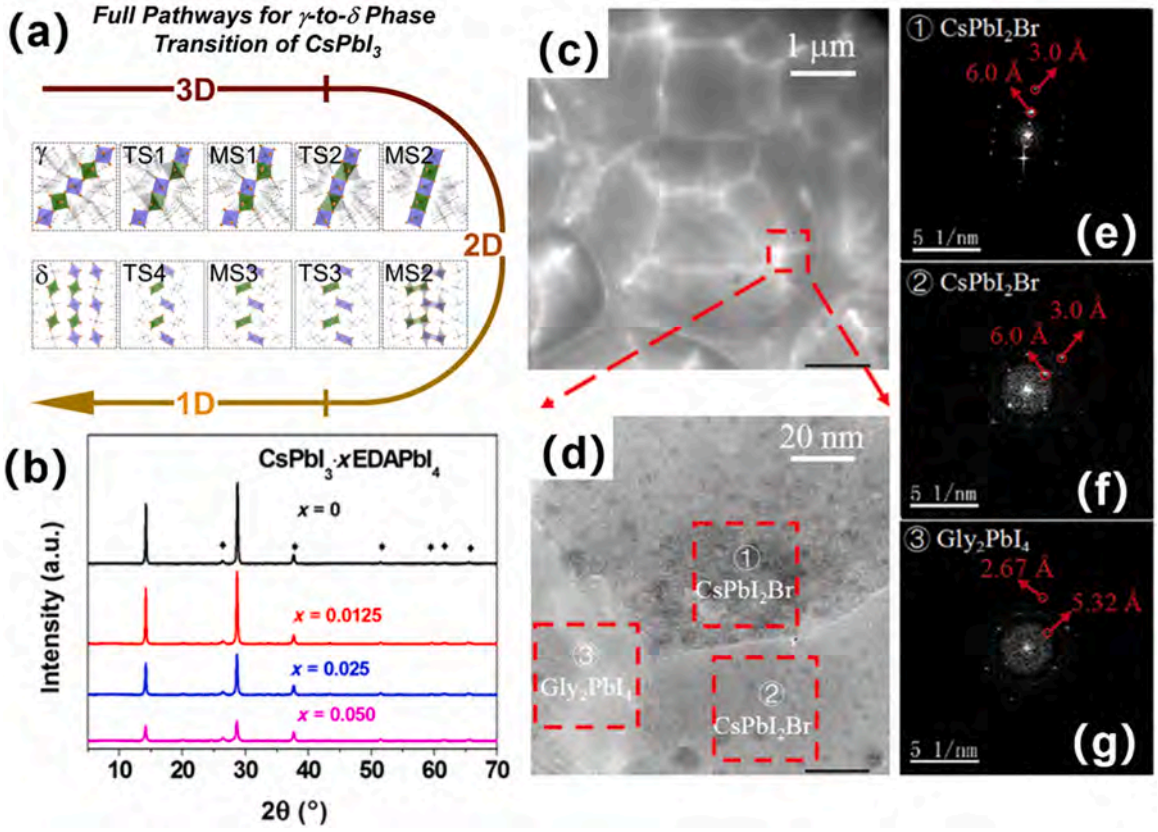

Fig. 4. The phase transition of $CsPbI_3$ from the perovskite γ phase to the non-perovskite δ phase proceeds through three intermediate states (MS1, MS2, and MS3) [45], and the existence of intermediate phases markedly reduces the threshold for phase transition. $EDAPbI_4$ is used to stabilize the Cs^+ perovskites, however the XRD analysis of $CsPbI_3$·x$EDAPbI_4$ samples revealed that no characteristic diffraction peaks corresponding to the $EDAPbI_4$ phase ($2\theta < 10°$) were observed [46]. Comparably, HRTEM analysis [47], $Cs_2PbI_2Cl_2$ was found to anchor onto $CsPbI_{2.5}Br_{0.5}$, with the (003) plane spacing of 2D $Cs_2PbI_2Cl_2$ measured at 6.16 Å and the (001) plane spacing of 3D $CsPbI_{2.5}Br_{0.5}$ measured at 6.06 Å. Permission to use the figures has been obtained from the Elsevier and John Wiley and Sons, and the corresponding Copyright Clearance Centers.

into MA-free bulk perovskites, and the resulting 2D components were embedded at the grain boundaries of the 3D bulk perovskite and distributed across half of the film thickness, effectively passivating defects. To promote the uniform distribution of 2D within the 3D phase, Zhou et al. [52] incorporated 1-naphthylmethylammonium iodide (NpMAI), which regulated the morphology of PbI_2 film and generated a porous structure, thereby facilitating diffusion of organic salts (FAI/MAI/MACl) into the PbI_2 film. The perovskite films controlled by $(NpMA)_2PbI_4$ exhibited significantly improved quality, with grain sizes increasing from ~500 nm to over 1000 nm, thus reducing grain boundary defects, extending carrier lifetimes, and suppressing ion diffusion.

Researchers have recognized that multi-cations perovskite systems inherently exhibit higher efficiency and longer stability than single-cation systems. Consequently, recent research has largely focused on multi-cations approaches. Continuous studies also indicate that a variety of organic cations, including phenylpropylammonium iodide (PPAI) with different alkyl chain lengths [53], pyrenylammonium iodides such as, pyrene-based 4,4',4'',4'''-(1,8-dihydropyrene-1,3,6,8-tetrayl)tetraaniline (TAPPy) [54], short-chain hydrophobic haloalkylammonium salts (2-chloroethylammonium, CEA^+, and 2-bromoethylammonium, BEA^+) [55], octane-1,8-diammonium (ODA) [56], aromatic formamidiniums (ArFA) [57], n-propylammonium iodide [32], 2-thiophenemethylammonium (ThMA) [23] and dodecylammonium chloride (DACl) [15], benefit the performance of multi-cations perovskite films, and the optimal performance of the multi-cation PSCs with a 2D component has reached 24.37 %. However, the identification of fully commercially viable and stable multi-cations systems remains to be established.

3.5. Sn based perovskite

Sn based perovskite, as the most promising lead-free perovskite materials, still face challenges in widespread application due to the facile oxidation of Sn^{2+} to Sn^{4+}. To inhibit the oxidation of Sn^{2+}, Yu et al. [58] replaced FA^+ with fluorophenylethylammonium bromide (FPEABr) in $FASnI_3$, and the FPEABr phase encapsulated the $FASnI_3$ grains, providing a reducing environment for the oxidation-prone 3D $FASnI_3$ grains. As a result, the well-known $Sn^{2+} \rightarrow Sn^{4+}$ oxidation was effectively suppressed. The commonly used PEAI [59] also benefits the suppress the $Sn^{2+} \rightarrow Sn^{4+}$ oxidation. Furthermore, Sanjay et al. [60] investigated the synergistic effect of PEAI and ethylenediamine diiodide ($EDAI_2$) on $FASnI_3$. They found the optimal ratio of the two additives was 8 mol% PEAI and 1 mol% $EDAI_2$, pinhole-free, dense perovskite films with excellent crystallinity and preferred orientation were obtained. The optimized devices achieved a stability for 5 days in ambient air without additional encapsulation.

In addition, several studies have focused on improving the phase stability of Sn-based perovskites by controlling their crystallization behavior. For example, Du et al. [61] synthesized and introduced 2D perovskite microcrystals of $3AMPYSnI_4$ ($3AMPY^{2+}$ represents 3-(aminomethyl)pyridinium) as seed crystals. The interaction between $3AMPY^{2+}$ and the Sn-I framework provided nucleation sites for the crystallization of the 3D parent perovskite and induced its epitaxial growth, resulting in perovskite films with larger and smoother grains. The Sn^{4+} content was reduced from 28.5 % to 8.4 %, indicating that oxidation was effectively suppressed. Kang et al. [62] introduced 4-guanidinobenzoic acid hydrochloride (GBAC) molecules, which induced the desorption of PEA from the perovskite surface and formed DMF-GBAC-SnI_2 hybrid chains. This process yielded a 2D and 3D mixed-phase film with a very low proportion of 2D phase, a dominant 3D phase, and high crystallinity, which benefit the phase stability under environment. Chang et al. [63] incorporated 4,4-difluoropiperidinium ($DFPD^+$) cations, which possess a high terminal positive charge density and strong coupling with the Sn-I framework. Through a one-step fabrication process, they constructed phase-pure $DFPD_2SnI_4$ and $FASnI_3$ mixed-phase perovskite films. The uniform distribution of $DFPD_2SnI_4$ along the 3D grain boundaries not only enhanced phase stability under environment but also effectively prevented carrier transport blockage. In fact, recent advances over the past two years in narrow-bandgap Sn-Pb perovskites have demonstrated that the incorporation of 2D components is highly effective in regulating the crystallization behavior of Sn-based perovskites [64,65]. Therefore, in order to obtain high-quality 2D and 3D mixed-phase Sn-based perovskites, it is of great significance to systematically explore and continuously investigate more suitable 2D components.

4. Optimization of structure for 2D and 3D mixed-phase perovskite

Beyond the aforementioned development of 2D materials, enhancing carrier transport at the interfaces of 2D and 3D mixed-phase perovskite is one of the critical research directions. Many 2D and 3D mixed-phase perovskites exist as localized heterojunctions at the surface and interface of the films. Under illumination, an internal electric field can be induced in the bulk of the solar cell. If the 2D/3D heterojunctions can participate in and facilitate carrier transport, device efficiency can be enhanced. Therefore, controlling the way 2D and 3D phases combined and establishing the correlation between their coupling modes and the device performance is another important research direction. The following discussion focuses on the latest advances in promoting carrier transport in 2D and 3D mixed-phase through additives and crystal orientation control, as well as the design of special 2D nanoplate-like structures within the 2D and 3D mixed-phase perovskite.

4.1. Additives to improve carrier transport

Although the incorporation of 2D perovskites into 3D perovskites can significantly enhance the intrinsic stability of the material, the carrier transport kinetics in the 2D component are often poor due to quantum and dielectric confinement effects [66]. To address this issue, additive engineering, through precise control of crystal growth, defect passivation, and interface optimization, has become a key strategy to overcome the efficiency and stability bottlenecks. Electron-acceptor molecule 1,2,4,5-tetracyanobenzene (TCNB) [67] and 1-naphthylmethylammonium (NMA) were introduced into the FA^{3+} perovskite to 2D and 3D mixed-phase film, denoted as PVK+NMAI and PVK+NMAI+TCNB. With high electron affinity, TCNB promotes electron transfer reactions and subsequently forms π_t–π_t interactions with NMA cations, which significantly increases lattice rigidity and reduces exciton binding energy. As shown in Fig. 5a, the lattice spacing of 3.18 Å corresponds to the (002) plane of cubic $FAPbI_3$, while the 7.38 Å spacing corresponds to the 2D perovskite, indicating that the 2D phase is mainly located at the grain boundaries of the 3D perovskite. Time-resolved PL (TRPL) fitting results (Fig. 5b) show that, compared to the pristine FA^+ film with a carrier lifetime of 538 ns, the PVK+NMAI and PVK+NMAI+TCNB films exhibit extended carrier lifetimes of 1686 ns and 2812 ns, respectively. Transient PL measurements (Fig. 5c) indicate that exciton lifetime increased from 2213 ps to 5711 ps. Based on dark *I-V* curves (Fig. 5d), the hole trap density decreased from 1.506×10^{16} cm^{-3} in the control film to 1.315×10^{16} cm^{-3} in PVK+NMAI, and further to 1.090×10^{16} cm^{-3} in PVK+NMAI+TCNB. As shown in Fig. 5f, compared to NMAI alone, the NMAI+TCNB system exhibits stronger binding on perovskite surfaces containing iodine vacancies or Pb-I antisite defects (Pb_I), indicating that TCNB facilitates NMAI adsorption on defect sites and thereby reduces defect density. Furthermore, to directly examine the influence of TCNB's strong electron-withdrawing capability on the perovskite work function, Kelvin probe force microscopy (KPFM) was employed. Since the work function is correlated with the contact potential difference (CPD), the CPD value can be used to directly evaluate the film work function. As shown in Fig. 5g-i the CPD decreases markedly upon TCNB incorporation, indicating an increased perovskite work function. This result confirms the occurrence of P-type

doping, which contributes to enhanced hole mobility. The energy-level diagram of the functional layer based on these results shows that the PVK+NMAI+TCNB film has the best energy alignment with spiro-OMeTAD, facilitating efficient hole extraction. Consequently, the device PCE is significantly improved to 24.01 %. Under unencapsulated conditions, the devices maintain approximately 94 % of their initial efficiency after exposure to ambient conditions for over 1000 hs. To address the inherent defect-induced limitations of carrier transport in Sn based perovskites [68], Jokar and colleagues [69] compared the effects of ethylenediammonium diiodide ($EDAI_2$) and BAI. They found that using only the BAI can enhance the crystallinity of $FASnI_3$ by modifying the crystal growth orientation, however, due to the imbalance between nucleation and growth rates, pinholes in the film could not be fully eliminated. By contrast, the addition of a small amount of $EDAI_2$ to the 2D precursor enables multi-site interactions between the diammonium cations and the perovskite, achieving a balanced nucleation-growth kinetic process, resulting in pinhole-free, dense films with enhanced carrier transport. Zheng et al. [70] synthesized a novel 2D and 3D mixed-phase perovskite film by doping small NH_4^+ cations. Theoretical calculations indicated that after NH_4^+ incorporation into the $FAPbI_3$ lattice, the initial 2D edge-sharing structure gradually evolved into a 2D and 3D mixed structure in kinetic simulations, with partial Pb-I bond breakage and formation of new bonds between layers, locally generating 3D structures. Devices fabricated from these films achieved a PCE of 18.25 % at n = 9, with negligible hysteresis. These results demonstrate that small molecule electron acceptors provide critical technological support for the commercialization of PSCs. Additionally, Lagher et al. [71] reported that the introduction of Cs^+ cations into perovskite components enhances photovoltaic performance with 27 % but reduces device stability. Consistently, Ali et al. [15] incorporated a small amount of CsI into a 2D and 3D mixed-phase precursor solution and observed that Cs^+ promotes 2D and 3D mixed-phase perovskite formation, corroborating Lagher's finding that Cs incorporation improves device efficiency.

4.2. *Regulating growth to achieve vertical orientation*

An important approach to enhancing the performance of 2D and 3D mixed-phase film is to increase the degree of vertical orientation of the heterostructure. When a large number of vertical quantum wells are effectively formed on the substrate, the 3D material acts as a high-speed carrier transport channel, while the 2D material forming the well walls serves as a barrier against external stimuli [72]. After spin-coating, the thickness of the perovskite precursor wet film can exceed several micrometers. At the microscopic scale, all solutes selectively grow around the nuclei. Many studies have attempted to use 2D materials as seeds to

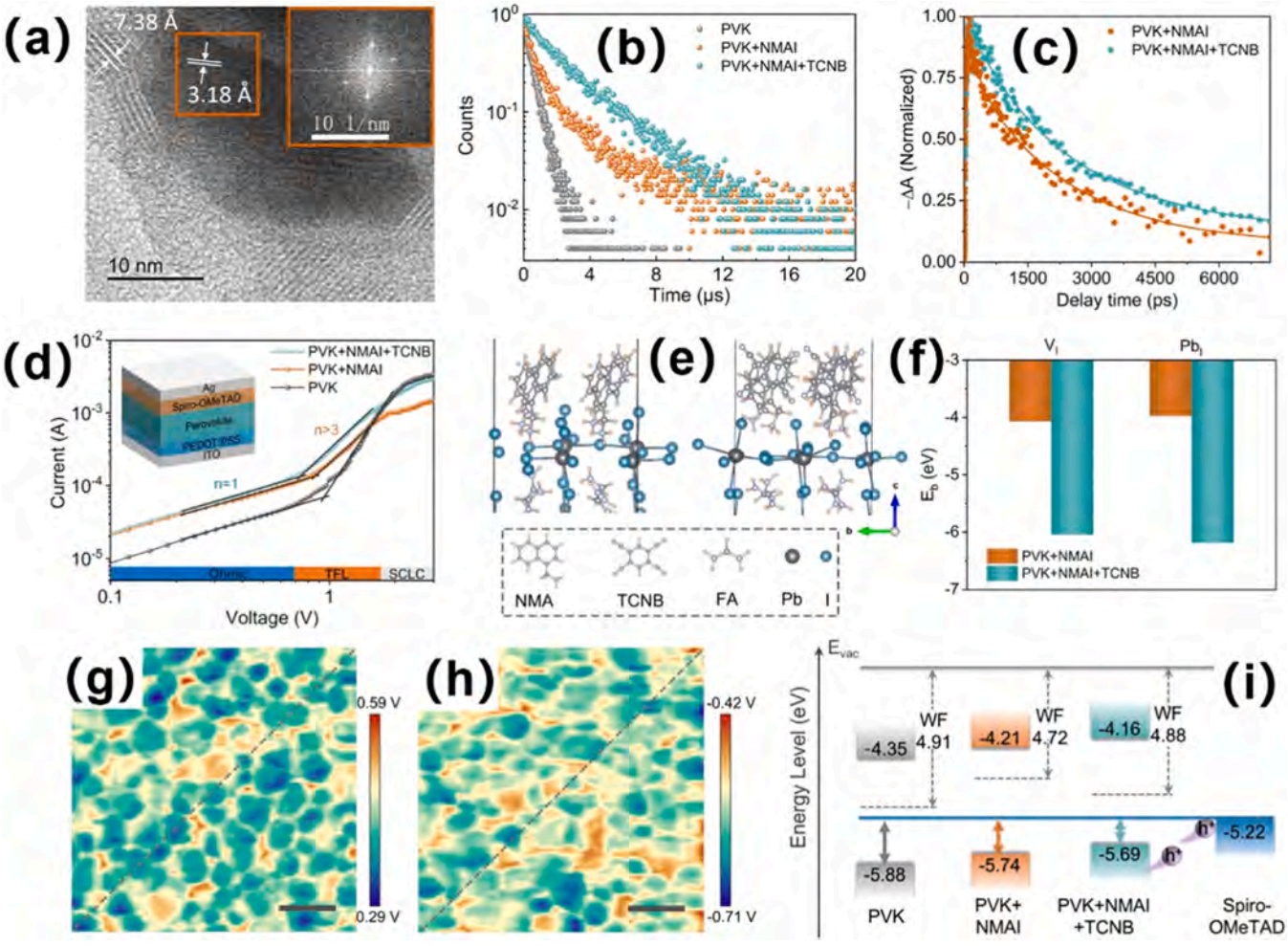

Fig. 5. Electron-acceptor molecule 1,2,4,5-tetracyanobenzene (TCNB) and 1-naphthylmethylammonium (NMA) were introduced into the FA^{3+} perovskite to form 2D and 3D mixed-phase film [67], denoted as PVK+NMAI and PVK+NMAI+TCNB. (a) HRTEM image of perovskite films containing NMAI and TCNB. (b) TRPL decay curves of the three perovskite films. (c) Recovery of the bleach signal as a function of delay time. (d) Dark *I-V* curves of hole-only devices and the device structure. (e) Optimized adsorption configurations of NMAI (left) and NMAI+TCNB (right) on the $FAPbI_3$ surface containing iodine vacancies. (f) Binding energies of NMAI and NMAI+TCNB on the defective $FAPbI_3$ surface. KPFM images of PVK+NMAI film (g) and PVK+NMAI+TCNB film (h) (scale bar: 2 μm). (i) Schematic energy-level diagram of the perovskite films. Permission to use the figures has been obtained from the John Wiley and Sons and the Copyright Clearance Center.

induce oriented growth of the 3D material. This is because: first, the layered structure of 2D perovskites, consisting of organic cations (e.g., BA^+, PEA^+) alternating with the inorganic $[Pb_6]^{4-}$ framework, is highly compatible with 3D perovskites; second, the interlayer spacing of 2D perovskites (~1.6 nm) and the in-plane lattice constant (a ≈ 6.3 Å) closely match those of 3D perovskites (e.g., $MAPbI_3$, a ≈ 6.2 Å), making 2D perovskites suitable as epitaxial growth templates [7,73]. Liu et al. [74] introduced an organic diamine spacer molecule, cystamine dihydrochloride (CysCl), into 3D perovskites to optimize the 3D crystal orientation, and reduce lattice distortion. Ye et al. [75] used an in-situ method to construct a highly oriented 2D@3D ($(AVA)_2PbI_4$@$MAPbI_3$) perovskite structure. Both of them achieved an improved PCE. Wang *et al.* [76] demonstrated that the halide composition in the 2D component also significantly influences the orientation of 3D crystals. By substituting halogens in PEA spacer cations to F, the better crystal orientation is achieved. Wu et al. [77] also reported by controlling crystallization to trigger the spontaneous reorientation of dipolar MA cations, a vertically polarized structure can be formed.

Zhou et al. [78] prepared tetrabutylammonium (TBA) based 2D and 3D mixed-phase perovskite, by using oriented 2D perovskite $(BDA)PbI_4$ as seeds to guide the crystallization of 3D perovskites, and excellent control over crystal plane orientation was achieved. In the detailed experiment, as shown in Fig. 6a, a series of highly mobile volatile salts (NH_4Cl, NH_4SCN, MASCN, and MACl) was introduced into the precursor solution, and orthogonal cation/anion combinations to elucidate the distinct contribution of each component to the optimization of 2D and 3D mixed-phase perovskite films was systematically compared. During TBA based 2D and 3D mixed-phase perovskites film formation, the volatile ions tend to leave the system while simultaneously driving the movement of other ions. This type of precursor system is thus defined as

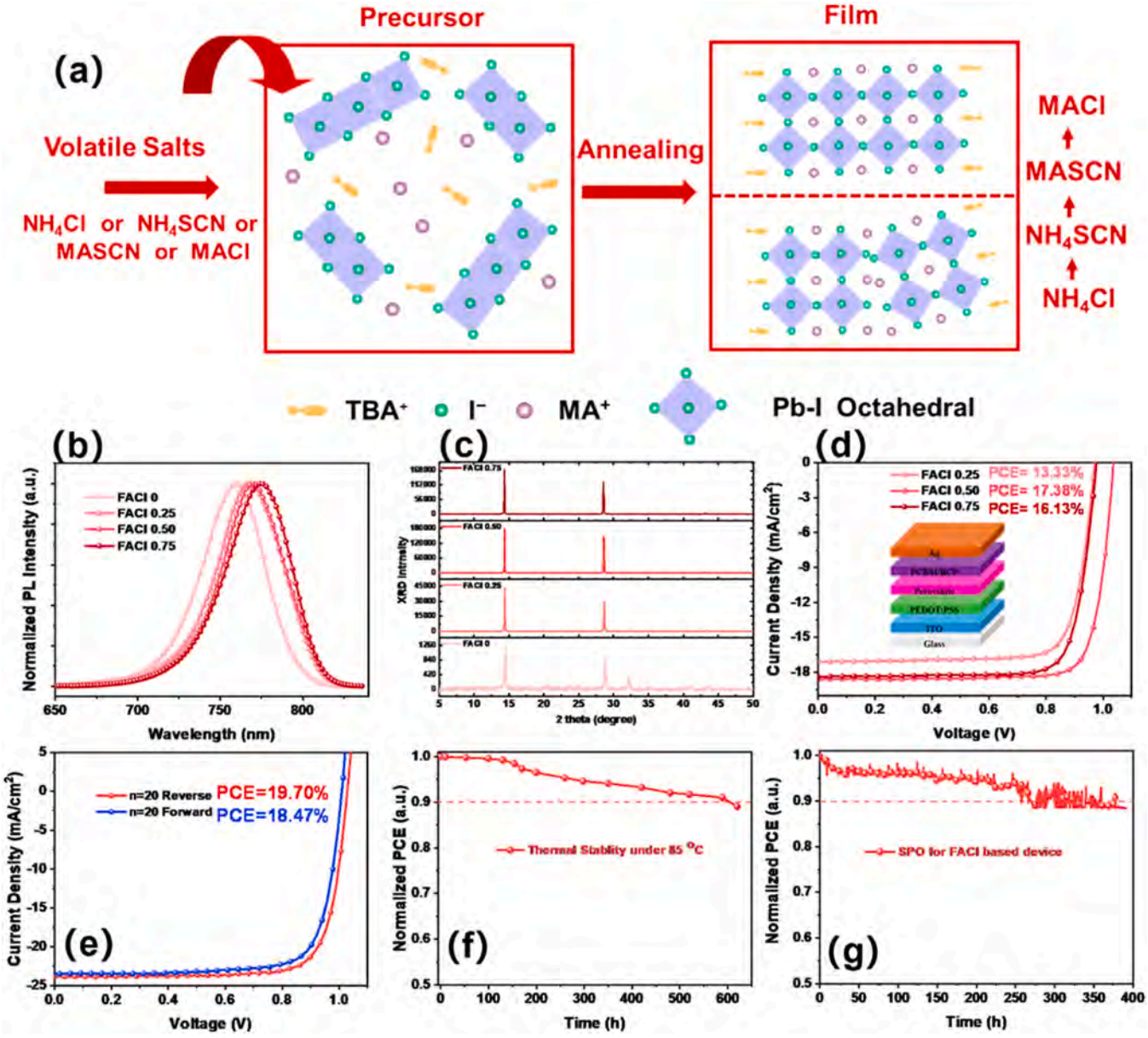

Fig. 6. A mechanism for the role of volatile small molecules in oriented crystal growth: due to their high mobility, these volatile salts can activate the precursor system and accelerate ion migration. During film formation, the volatile ionic salts tend to escape from the system, simultaneously driving the movement of other ions (a). All the volatile salts used in this study could significantly enhance the crystallinity and crystal orientation of TBA-based perovskite films. Additionally, $TBA_2(FA_aMA_{1-a})_{n-1}Pb_nI_{3n+1}$ was constructed, and by adjusting the FACl/MAI ratio, they demonstrated corresponding results in PL (b), XRD (c), device PCE (d and e), and stability (f and g) [78]. Permission to use the figures has been obtained from the American Chemical Society the Copyright Clearance Center.

a "mobile media". The authors found that all volatile salts significantly enhanced the crystallinity and crystal orientation of the TBA based perovskite films. To further optimize optoelectronic performance, MACl was replaced with FACl as the volatile component to construct $TBA_2(FA_aMA_{1-a})_{n-1}Pb_nI_{3n+1}$. By adjusting the FACl/MAI ratio, the PL emission peak gradually red-shifted from 760 nm to 766 nm ($FACl_{0.25}$), 770 nm ($FACl_{0.5}$), and 776 nm ($FACl_{0.75}$), indicating effective bandgap modulation (Fig. 6b). XRD results (Fig. 6c) showed that with increasing FA^+ content in $TBA_2MA_9Pb_{10}I_{31}$, diffraction peaks gradually shifted to lower angles. Optimized solar cell with different FACl contents are shown in Fig. 6d, with PCEs in the order of $FACl_{0.25}$ (13.33 %) < $FACl_{0.75}$ (16.13 %) < $FACl_{0.5}$ (17.38 %), indicating that $FACl_{0.5}$-assisted perovskite films deliver the best device performance. Furthermore, high-n-value (n = 20) $TBA_2MA_{19}Pb_{20}I_{61}$ perovskite devices exhibited PCEs of 19.70 % (reverse scan) and 18.47 % (forward scan) (Fig. 6e), among the highest for all 2D and 3D mixed-phase PSCs. Device stability tests showed that under continuous LED illumination at room temperature in a N_2 glovebox, devices retained 90 % of the initial efficiency after 350 h (Fig. 6f). Additionally, FACl-based PSCs maintained 92 % of the initial PCE after 500 h of thermal storage at 85 °C under unencapsulated conditions and subsequent testing under one-sun illumination at room temperature (Fig. 6g), demonstrating excellent operational durability and thermal stability.

Beyond basic oriented growth, selective control of specific crystal facets in perovskite crystals represents another important research direction. Different crystal orientations correspond to significant differences in facet-specific defect densities, which directly affect charge separation and recombination processes [79], and thereby lead to variations in device performance. For example, the (100) facet exhibits a dense atomic arrangement and relatively low surface energy [80], resulting in the lowest defect density. This is conducive to efficient charge extraction, enabling long carrier diffusion lengths (over 1 μm) and low nonradiative recombination rates. Consequently, perovskite films dominated by (100)-oriented crystals can achieve PCEs exceeding 23 % with V_{oc} losses as low as 0.3 V. In contrast, the (111) facet, with higher surface energy, is prone to forming iodine vacancies, dislocations, and lattice distortions, leading to significantly higher defect densities and noticeable *I-V* hysteresis. Devices dominated by (111)-oriented crystals typically have efficiencies below 20 %, V_{oc} losses exceeding 0.5 V, and their long-term operational stability is severely compromised due to the high defect density and enhanced ion migration. Yang *et al.* [81] deliberately suppressed the dynamic preferential growth of the (111) facet by controlling the selective adsorption of ammonium halide additives on different perovskite facets, while allowing a small amount of (202) facets to serve as secondary nucleation sites, promoting the formation of large grains. As the halide-regulated deprotonation of the ammonium salts proceeded, the (111) facet gradually regained its growth dominance, ultimately forming vertically oriented 2D perovskite films with high uniformity, reduced defect density, and ideal carrier transport/collection kinetics.

Although the introduction of 2D perovskites in solution-processed systems can guide crystal growth, the complex crystallization kinetics during the solution-to-solid phase transition pose significant challenges for practical applications. The interplay between solvent evaporation rate and nucleation barriers can trigger rapid, non-equilibrium crystallization, resulting in highly polydisperse grain size distributions and high grain boundary densities. In addition, solution flows dominated by the Marangoni effect exacerbate the coffee-ring effect, while incomplete stress relaxation during crystallization introduces defects such as pinholes and microcracks. These uncontrollable crystal growth phenomena significantly increase the film defect density, severely limiting both the power conversion efficiency and long-term stability of the devices [82]. Therefore, much more effort should focus on precise control of crystallization kinetics in solution-processed systems.

4.3. 2D phase existing as nanoplates

The 2D phase exists as nanoplates is another type of 2D and 3D mixed-phase perovskite films. Wang et al. [12] precisely controlling the BA content, they obtained plate-like layered perovskite crystals oriented perpendicular to the 3D film plane. These plate-like crystals were embedded between 3D perovskite grains, forming a stable heterostructure. Solar cells containing the optimally doped BA cations achieved an average stable PCE of 17.5 ± 1.3 % for 1.61 eV bandgap perovskites and 15.8 ± 0.8 % for 1.72 eV bandgap perovskites. In the research by Hu et al. [83] hydrophobic $MA_3Bi_2I_9$ nanosheets were vertically distributed between $MAPbI_3$ crystals. Solar cells based on this heterostructure film achieved a high PCE of 18.97 %, with significantly reduced hysteresis and greatly enhanced stability. PEAI-based perovskite nanosheets [84] is also embed into a 3D $FA_{0.95}Cs_{0.05}PbI_3$ matrix. SEM images showed that the nanosheet preferentially oriented perpendicular to the substrate, forming a highly ordered composite film structure that ensured continuous charge transport pathways. The resulting films exhibited electron and hole mobilities (>100 $cm^2/(V{\cdot}s)$) comparable to pure 3D perovskites, while maintaining a PCE above 20 %, approaching the theoretical limit for single-junction perovskite devices.

In addition to the mainstream optimization strategies mentioned above, there are still some important and emerging research topics aimed at further improving the performance of 2D and 3D mixed-phase perovskite films, such as: (1) suppress ion migration across the 2D/3D interface. Cation migration between 2D and 3D layers can disrupt the octahedral network, leading to performance degradation over time. Liu et al. [85] reported a perovskite material $(A_6BfP)_9PbI_{22}$ (A_6BfP refers to N-aminohexyl-benz[*f*]-phthalimide) forming a robust organic-inorganic network through edge-sharing and face-sharing. This perovskite-perovskite heterostructure effectively suppresses cation migration, and encapsulated large-area devices maintained excellent stability at 85°C in air for 1250 hs. (2) uncover carrier transport mechanisms between 2D and 3D perovskite films. Existing models include [86]: (Model I) There exists a gradual dimensional transition along the axial direction, and the 2D and 3D mixed-phase exhibit type-II band alignment, which favors global carrier separation. (Model II) 2D perovskite fragments are dispersed in the 3D perovskite matrix with macroscopic axial concentration variations. Yu et al. [87] proposed a more accurate model that considers both (Model I) the interspersed distribution of phases and (Model II) the 2D/3D heterojunction as a p-n junction with built-in potential, emphasizing that the 2D/3D interface is the key factor limiting charge transport. (3) Ambiguity in the understanding of 2D materials within 2D and 3D mixed-phase perovskites. Although 3D perovskites can be "sliced" into layered structures using organic cations of different lengths, the dimensionality of these layers is not absolute. Some may form "quasi-2D" structures between 2D and 3D, and whether they are considered 2D affects the understanding of their optical and electrical properties as well as device design strategies [88]. Meanwhile, from the perspective of the entire device, the carrier transport properties of other functional layers and their compatibility with 2D and 3D mixed-phase perovskite films should also be given attention. For example, studies on 3D perovskite films have shown that significantly increasing the electron mobility of the electron transport layer by 2–3 orders of magnitude [89,90] or enhancing the conductivity of the hole transport layer through sufficient oxidation [91] can markedly improve the efficiency and stability of 3D devices. Similarly, 2D and 3D mixed-phase perovskite films also require electron and hole transport layers that are well-matched to their properties.

5. Characterization for the 2D and 3D mixed-phase perovskite film

SEM, XRD and grazing-incidence wide-angle X-ray scattering (GIWAXS) are the most direct and common method to observe the

structural characteristics of 2D phases within a 3D perovskite matrix [12,84,92]. Zhou *et al.* [23] identified the 2D phase and the 3D phase using SEM, XRD, and GIWAXS. Fig. 7a and 7b show top-view SEM images of pure 3D perovskite films and 2D and 3D mixed-phase perovskite films. They found that the grain size of pure 3D perovskite films is relatively small, while the grain size of 2D and 3D mixed-phase films is significantly larger. XRD characterization (Fig. 7c) revealed that 2D and 3D perovskite films display clear and sharp characteristic diffraction peaks, with preferred (110) and (202) orientations. Compared with pure 3D perovskite films, the main perovskite peak around 14° in the 2D and 3D films slightly shifts to higher angles, indicating that 2D cations have been incorporated into the 3D perovskite lattice. However, conventional XRD results also show that no new diffraction peaks appear at small angles ($2\theta < 12°$) even for 2D and 3D mixed-phase perovskite films. GIWAXS analysis (Fig. 7d and e) further showed that pure 3D perovskite films exhibit the typical features of a 3D perovskite structure, i.e., broad Debye-Scherrer rings with relatively uniform azimuthal intensity distribution, indicating isotropic grain orientation. In contrast, 2D and 3D mixed-phase perovskite films exhibit higher diffraction intensity accompanied by sharp and discrete Bragg spots, indicating partial grain reorientation during the formation of the 2D and 3D mixed-phase layer. Comparatively, it is evident that GIWAXS is more sensitive to structural changes in 2D and 3D mixed-phase perovskite films, whereas SEM and XRD require a comprehensive assessment depending on the specific circumstances.

Beyond the aforementioned conventional characterization approaches, additional techniques are available to investigate specific physical processes occurring within the device. Transient absorption (TA) spectroscopy was used to track carrier dynamics [87], revealing the distinctive role of the 2D connectors that enabled carrier migration in the dark but formed transport barriers under illumination. Ultraviolet photoelectron spectroscopy (UPS) of electronic energy levels were used to indicate that this phenomenon originates from an enhanced built-in potential induced by interface trap filling. To challenge the traditional notion of a "gradual dimensional transition", two-photon PL mapping and time-of-flight secondary ion mass spectrometry (TOF-SIMS) were used to visualize nanoscale disordered phase distributions. This clearly identified the core issue that in-plane carrier blocking effect leads to reduced J_{sc} and FF. To investigate the practical issue of "thermal stability" in 2D and 3D mixed-phase perovskite films [93], in situ GIWAXS was employed to monitor structural changes during thermal cycling, as shown in Fig. 7f, confirming that the 2D layer protects the 3D bulk diffraction peaks from attenuation.

In the research progress of 2D and 3D mixed-phase perovskite films, establishing a comprehensive research framework-spanning from mechanistic analysis to structural regulation, practical stability verification, and core defect mitigation-still relies heavily on versatile characterization techniques that can operate across multiple dimensions and adapt to diverse research objectives. The synergistic integration of these techniques has become critical drivers of breakthroughs at each stage of research. For example, Zhi et al. [94] conducted an in-depth investigation into defect control within $FAPbI_3$. Ultra-low-dose transmission electron microscopy (ULD-TEM) and selected-area electron diffraction (SAED) were employed to directly observe the evolution of defects, clearly revealing the presence of high-density in-plane defects in pristine $FAPbI_3$, a reduction in defect density after the introduction of PEA_2PbI_4, and complete defect elimination upon further incorporation of MACl. SEM and atomic force microscopy (AFM) further confirmed that the co-addition samples exhibited larger grain sizes and smoother surfaces. To gain deeper insights into the crystal structure and lattice strain, XRD combined with Williamson-Hall (WH) analysis was performed, indicating that PEA_2PbI_4 does not enter the $FAPbI_3$ lattice, whereas MA^+ ions

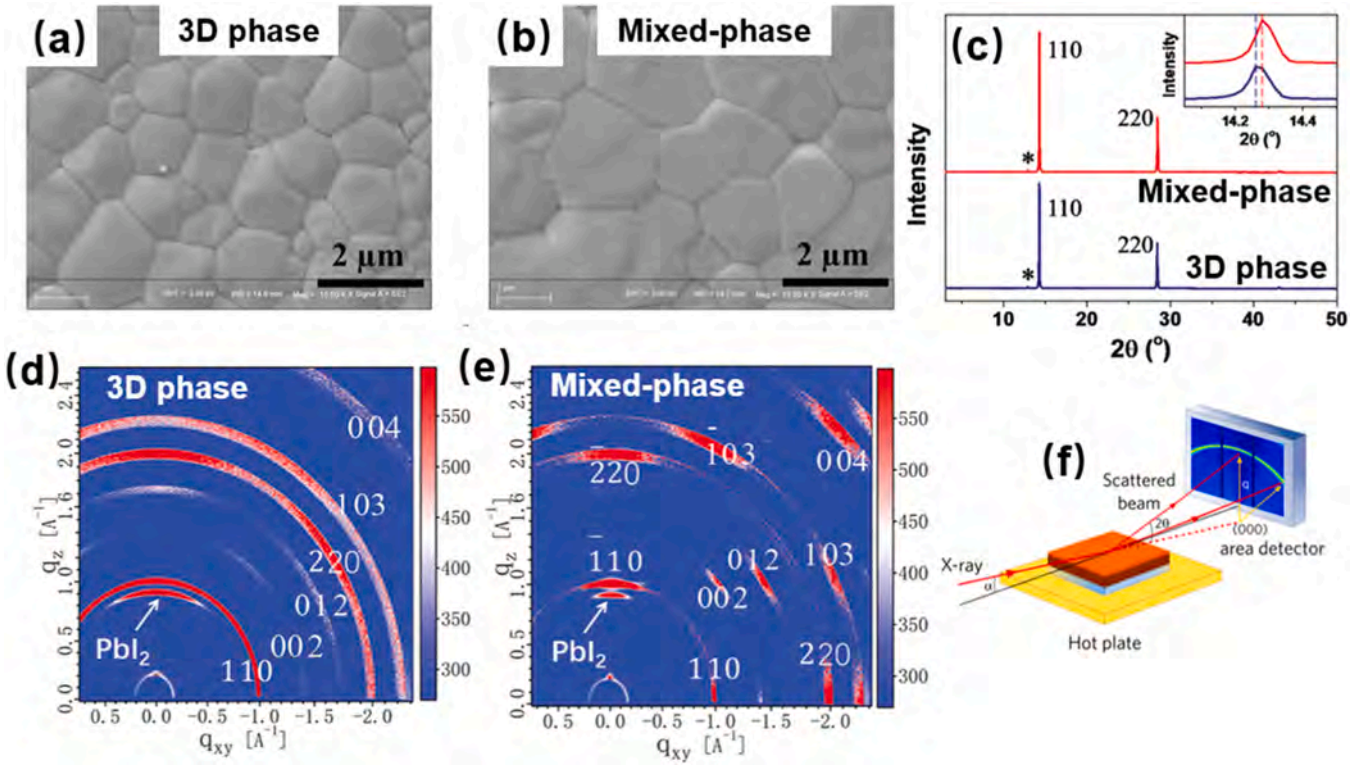

Fig. 7. presents a comparison of conventional analyses of the microstructure, phase, and orientation distribution of pure 3D perovskite films and 2D and 3D mixed-phase perovskite films. SEM images (a and b) show that introducing 2D components into 3D perovskites significantly alters the surface morphology, particularly the grain size. XRD patterns (c) indicate that, although the overall crystal structure largely retains the 3D main phase, the d-spacing of certain crystal planes can slightly increase. GIWAXS patterns (d and e) reveal that while pure 3D films typically exhibit continuous diffraction rings, the addition of 2D components results in discrete diffraction spots [23]. It also presents the in situ XRD monitoring of the thermal degradation process of the perovskite films (f) [93]. Permission to use the figures has been obtained from the John Wiley and Sons and the Copyright Clearance Centers.

from MACl can be incorporated into the lattice. PL, photoluminescence quantum yield (PLQY), TRPL, and femtosecond pump-probe transient absorption (TA) spectroscopy verified defect elimination from the perspective of carrier dynamics. Space-charge-limited current (SCLC) measurements further confirmed that the co-addition samples possessed the lowest trap density. Finally, comprehensive analyses of current-voltage characteristics, external quantum efficiency (EQE), Urbach energy, and stability tests demonstrated that the co-addition devices achieved a PCE of 23.69 % with markedly enhanced stability. This systematic integration and application of multiple characterization techniques provide valuable insights into defect regulation in 2D and 3D mixed-phase perovskite.

6. Conclusion

3D PSCs exhibit broad application prospects in post-silicon photovoltaic systems. However, despite their excellent efficiency performance, their stability remains relatively poor. Studies have shown that reducing the dimensionality of the 3D component to 2D can significantly improve its instability, which has led to expectations that 2D and 3D mixed-phase PSCs could achieve both high durability and high efficiency. In this review, we present methods for preparing 2D and 3D mixed-phase films. Among these, the one-step and two-step solution methods are improvements over classic 3D film fabrication techniques, while the ITC method has recently been proposed as a new approach to reduce defects in perovskite films. We further categorize the recent development of new 2D materials according to the parent perovskite components: MA^+, FA^+, Cs^+, multi-cations, and Sn-based perovskites. Unfortunately, there are currently no comparative studies on the performance of the same 2D material across different 3D perovskite matrix. Moreover, we summarize current directions for structural and performance optimization of 2D and 3D mixed-phase perovskite films, including: improving carrier transport via additives, achieving oriented growth of the 2D phase through crystallization control, and utilizing the unique nanoplate structure of the 2D phase for performance enhancement. Finally, we review methods for identifying 2D structures within 2D and 3D mixed-phase using conventional morphology, phase, and performance characterization, as well as system-level characterization techniques for probing special physical phenomena. This review aims to help researchers gain a deeper understanding of the impact of dimensional reduction on PSCs from multiple perspectives: synthesizing 2D and 3D mixed-phase films, developing targeted 2D materials, continuously optimizing 2D and 3D mixed-phase films, and developing new characterization methods. Such insights can guide the adjustment and improvement of research objectives, ultimately supporting the development of high-performance, commercially viable PSCs.

CRediT authorship contribution statement

Jenny Flores Garcia: Methodology. **Weiwu Dang:** Methodology, Investigation. **Teresa Gatti:** Project administration. **Xiaolan Li:** Writing – original draft, Visualization, Methodology, Investigation, Conceptualization. **Yan Li:** Writing – review & editing, Writing – original draft, Visualization, Validation, Supervision, Project administration, Methodology, Investigation, Funding acquisition, Formal analysis, Conceptualization. **Hong He:** Writing – original draft, Methodology, Investigation. **Haoxu Wang:** Methodology, Investigation. **Jianhua Chen:** Methodology, Investigation. **Xian Gu:** Methodology, Investigation. **Zhao Li:** Validation, Supervision.

Declaration of Competing Interest

This work is original, unpublished, and not being considered for publication elsewhere. Its publication is approved by all authors and the responsible authorities. All authors declare no conflict of interest.

Acknowledgements

National Natural Science Foundation of China (Grant No. 62204202); Natural Science Basic Research Program of Shaanxi Province (Grant No. 2024JC-YBMS-438 and 2025JC-YBMS-420); The Key Research and Development Program of Shaanxi Program (Grant No. 2023KXJ-172); 2024 Scientific Research Project of Shaanxi Institute of technology (Grant No. Gfy24-04); T.G. acknowledges financial support from the European Research Council for the project JANUS BI (grant agreement no. [101041229])

Data Availability

No data was used for the research described in the article.

References

[1] T. Oku, Crystal structures of perovskite halide compounds used for solar cells, Rev. Adv. Mater. Sci. 59 (1) (2020) 264–305.
[2] National Renewable Energy Laboratory, Best Research Cell Efficiencies, ⟨https://www.nrel.gov/pv/cell-efficiency.html⟩.
[3] T.M. Koh, K. Thirumal, H.S. Soo, N. Mathews, Multidimensional perovskites: a mixed cation approach towards ambient stable and tunable perovskite photovoltaics, ChemSusChem 9 (18) (2016) 2541–2558.
[4] S.G. Cao, Z.E. Bi, T.J. Zheng, S.Z. Luo, L.G. Gutsev, B.R. Ramachandran, V. V. Ozerova, N.A. Emelianov, N.A. Slesarenko, Y.P. Zheng, B.Z. Taye, G.L. Gutsev, S. M. Aldoshin, P.A. Troshin, X.Q. Xu, Revealing interaction of fluorinated propylamine hydrochloride with precursor and defect states of perovskite films toward efficient flexible solar cells, Adv. Funct. Mater. 34 (42) (2024) 2405078.
[5] X.T. Li, J.M. Hoffman, M.G. Kanatzidis, The 2D halide perovskite rulebook: how the spacer influences everything from the structure to optoelectronic device efficiency, Chem. Rev. 121 (4) (2021) 2230–2291.
[6] C.M.M. Soe, C.C. Stoumpos, M. Kepenekian, B. Traoré, H. Tsai, W.Y. Nie, B. H. Wang, C. Katan, R. Seshadri, A.D. Mohite, J. Eyen, T.J. Marks, M.G. Kanatzidis, New type of 2D perovskites with alternating cations in the interlayer space, $(C(NH_2)_3)(CH_3NH_3Pb_nI_{3n+1}$: structure, properties, and photovoltaic performance, J. Am. Chem. Soc. 139 (45) (2017) 16297–16309.
[7] Y.K. Xu, M. Wang, Y.T. Lei, Z.P. Ci, Z.W. Jin, Crystallization kinetics in 2D perovskite solar cells, Adv. Energy Mater. 10 (43) (2020) 2002558.
[8] Q.H. Li, L. Zhou, T. Zhou, Fluorinated quasi 2D perovskite solar cells with improved stability and over 19% efficiency, Adv. Energy Mater. 14 (22) (2024) 2400050.
[9] Y.N. Chen, Y. Sun, J.J. Peng, J.H. Tang, K.B. Zheng, Z.Q. Liang, 2D ruddlesden-popper perovskites for optoelectronics, Adv. Mater. 30 (2) (2018) 1703487.
[10] G. Grancini, C. Roldán-Carmona, I. Zimmermann, E. Mosconi, X. Lee, D. Martineau, S. Narbey, F. Oswald, F. De Angelis, M. Graetzel, M.K. Nazeeruddin, One-year stable perovskite solar cells by 2D/3D interface engineering, Nat. Commun. 8 (2017) 15684.
[11] E.D. Kinigstein, H. Tsai, W.Y. Nie, J.C. Blancon, K.G. Yager, K. Appavoo, J. Even, M.G. Kanatzidis, A.D. Mohite, M.Y. Sfeir, Edge states drive exciton dissociation in ruddlesden-popper lead halide perovskite thin films, ACS Mater. Lett. 2 (10) (2020) 1360–1367.
[12] Z.P. Wang, Q.Q. Lin, F.P. Chmiel, N. Sakai, L.M. Herz, H.J. Snaith, Efficient ambient-air-stable solar cells with 2D-3D heterostructured butylammonium-caesium-formamidinium lead halide perovskites, Nat. Energy 2 (9) (2017) 17135.
[13] A.C. Janetos, Energy infrastructure: mapping future electricity demand, Nat. Energy 1 (2016) 16116.
[14] M.A. Mahmud, T. Duong, J. Peng, Y.L. Wu, H.P. Shen, D. Walter, H.T. Nguyen, N. Mozaffari, G.D. Tabi, K.R. Catchpole, K.J. Weber, T.P. White, Origin of efficiency and stability enhancement in high-performing mixed dimensional 2D-3D perovskite solar cells: a review, Adv. Funct. Mater. 32 (3) (2022) 2009164.
[15] N. Ali, X.Y. Wang, S. Rauf, S. Attique, A. Khesro, S. Ali, N. Mushtaq, H.B. Xiao, C. P. Yang, H.Z. Wu, Enhanced stability in cesium assisted hybrid 2D/3D-perovskite thin films and solar cells prepared in ambient humidity, Sol. Energy 189 (2019) 325–332.
[16] H. Gao, C.X. Ban, F.M. Li, T. Yu, J. Yang, W.D. Zhu, X.X. Zhou, G. Fu, Z.G. Zou, Nucleation and crystal growth of organic-inorganic lead halide perovskites under different relative humidity, ACS Appl. Mater. Inter. 7 (17) (2015) 9110–9117.
[17] J.G. Sun, X.L. Zhang, X.F. Ling, Y.G. Yang, Y. Wang, J.J. Guo, S.Z. Liu, J.Y. Yuan, W.L. Ma, A penetrated 2D/3D hybrid heterojunction for high-performance perovskite solar cells, J. Mater. Chem. A 9 (40) (2021) 23019–23027.
[18] Y.Q. Zou, Y. Cui, H.Y. Wang, Q.B. Cai, C. Mu, J.P. Zhang, Highly efficient and stable 2D 3D perovskite solar cells fabricated by interfacial modification, Nanotechnology 30 (27) (2019) 275202.
[19] J.W. Li, M.G. Wu, G.J. Yang, D.Y. Zhang, Z.J. Wang, D. Zheng, J.S. Yu, Bottom-up passivation effects by using 3D/2D mix structure for high performance p-i-n perovskite solar cells, Sol. Energy 205 (2020) 44–50.
[20] W.J. Zou, L.T. Shan, W.C. Cao, J. Chen, X. Liu, J.S. Yu, L. Shen, K. Yao, Precrystallized-Heterojunction strategy on precursor solution enables high-performance semitransparent perovskite solar cells, Adv. Opt. Mater. 11 (12) (2023) 2202982.

[21] D. Zhang, X.F. Wang, Z.P. Fan, Y.X. Zhao, X.F. Xia, F. Li, In situ-grown 2D perovskite based on π-conjugated aggregation-induced emission organic spacer boosting the efficiency and stability of 2D-3D heterostructured perovskite solar cells, ACS Appl. Mater. Inter. 16 (10) (2024) 12833–12843.

[22] M. Younas, M.A. Gondal, M.A. Dastageer, Fabrication of perovskite solar cells using novel 2D/3D-blended perovskite single crystals, Int. J. Energy Res. 45 (4) (2021) 5555–5566.

[23] T. Zhou, H.T. Lai, T.T. Liu, D. Lu, X.J. Wan, X.D. Zhang, Y.S. Liu, Y.S. Chen, Highly efficient and stable solar cells based on crystalline oriented 2D/3D hybrid perovskite, Adv. Mater. 31 (32) (2019) 1901242.

[24] J. Xiang, F. Wang, X. Liang, D.W. Duan, M.J. Yuan, T.M. Wu, H.L. Hu, Y.M. Shi, Phase transitions in mixed-dimensional perovskite: from film formation evolution to its impact on optoelectronic properties, Chem. Eng. J. 500 (2024) 157369.

[25] M.L. Li, Y.M. Xie, X.W. Xu, Y.P. Huo, S. Tsang, Q.D. Yang, Y.H. Cheng, Comparison of processing windows and electronic properties between $CH_3NH_3PbI_3$ perovskite fabricated by one-step and two-step solution processes, Org. Electron 63 (2018) 159–165.

[26] Y. Huang, L. Li, Z. Liu, H. Jiao, Y. He, X. Wang, R. Zhu, D. Wang, J. Sun, Q. Chen, H. Zhou, The intrinsic properties of $FA_{(1-x)}MA_xPbI_3$ perovskite single crystals, J. Mater. Chem. A 5 (18) (2017) 8537–8544.

[27] X.Y. Chen, M.M. Ding, T.Y. Luo, T. Ye, C.Y. Zhao, Y.N. Zhao, W.F. Zhang, H. X. Chang, Self-Assembly of 2D/3D perovskites by crystal engineering for efficient air-processed, air-stable inverted planar perovskite solar cells, ACS Appl. Energy Mater. 3 (3) (2020) 2975–2982.

[28] Y. Zou, Y.P. Gao, Y.S. Liu, The role of organic spacers in 2D/3D hybrid perovskite solar cells, Mater. Chem. Front 8 (1) (2023) 82–103.

[29] Y.R. Li, J.W. Wu, Y. Zhang, L.Z. Zhang, X.Y. Zhou, B.H. Hu, Z.Y. Jiang, J. Zeng, D. Y. Wang, Y.L. Liu, S. Chen, Z.X. Liu, C. Liu, X.Z. Wang, B.M. Xu, Whether organic spacer cations induced 2D/3D or quasi-2D/3D mixed dimensional perovskites? Chem. Eng. J. 450 (2022) 137887.

[30] X.Q. Jiang, J.F. Zhang, X.T. Liu, Z.Y. Wang, X. Guo, C. Li, Deeper insight into the role of organic ammonium cations in reducing surface defects of the perovskite film, Angew. Chem. Int. Ed. 61 (12) (2022) e202115663.

[31] F. Schmitz, J. Horn, N. Dengo, A.E. Sedykh, J. Becker, E. Maiworm, P. Bélteky, A. Kukovecz, S. Gross, F. Lamberti, K. Müller-Buschbaum, D. Schlettwein, D. Meggiolaro, M. Righetto, T. Gatti, Large cation engineering in two-dimensional silver-bismuth bromide double perovskites, Chem. Mater. 33 (12) (2021) 4688–4700.

[32] D.S. Yao, C.M. Zhang, S.L. Zhang, Y. Yang, A.J. Du, E. Waclawik, X.C. Yu, G. J. Wilson, H.X. Wang, 2D-3D mixed organic-inorganic perovskite layers for solar cells with enhanced efficiency and stability induced by n-propylammonium iodide additives, ACS Appl. Mater. Inter. 11 (33) (2019) 29753–29764.

[33] Y. Li, J.H. Zhang, J. Xiang, H.L. Hu, H.Z. Zhong, Y.M. Shi, A Novel 4,4'-bipiperidine-based organic salt for efficient and stable 2D-3D perovskite solar cells, ACS Appl. Mater. Inter. 14 (19) (2022) 22324–22331.

[34] M.S. de Holanda, R. Szostak, P.E. Marchezi, L. Duarte, J.C. Germino, T.D.Z. Atvars, A.F. Nogueira, In situ 2D perovskite formation and the impact of the 2D/3D structures on performance and stability of perovskite solar cells, Sol. RRL 3 (9) (2019) 1900199.

[35] S. Chen, N. Shen, L.H. Zhang, L.Z. Zhang, S.H. Cheung, S.M. Chen, S.K. So, B.M. Xu, Understanding the interplay of binary organic spacer in ruddlesden-popper perovskites toward efficient and stable solar cells, Adv. Funct. Mater. 30 (10) (2020) 1907759.

[36] X. Huang, Q.H. Cui, W.T. Bi, L. Li, P.C. Jia, Y.B. Hou, Y.F. Hu, Z.D. Lou, F. Teng, Two-dimensional additive diethylammonium iodide promoting crystal growth for efficient and stable perovskite solar cells, RSC Adv. 9 (14) (2019) 7984–7991.

[37] B.P. Nguyen, J. Kim, H.K. Park, W. Jo, G.Y. Kim, Enhanced charge transport via mixed-dimensional heterostructures in 2D-3D perovskites and their relevance to solar cells, ACS Appl. Energy Mater. 5 (7) (2022) 7965–7976.

[38] T.M. Koh, V. Shanmugam, X.T. Guo, S.S. Lim, O. Filonik, E.M. Herzig, P. Müller-Buschbaum, V. Swamy, S.T. Chien, S.G. Mhaisalkar, N. Mathews, Enhancing moisture tolerance in efficient hybrid 3D/2D perovskite photovoltaics, J. Mater. Chem. A 6 (5) (2018) 2122–2128.

[39] G.E. Eperon, S.D. Stranks, C. Menelaou, M.B. Johnston, L.M. Herz, H.J. Snaith, Formamidinium lead trihalide: a broadly tunable perovskite for efficient planar heterojunction solar cells, Energy Environ. Sci. 7 (3) (2014) 982–988.

[40] N.J. Jeon, J.H. Noh, W.S. Yang, Y.C. Kim, S. Ryu, J. Seo, S.I. Seok, Compositional engineering of perovskite materials for high-performance solar cells, Nature 517 (7535) (2015) 476–480.

[41] T.H. Yang, C. Ma, W.L. Cai, S.Q. Wang, Y. Wu, J.S. Feng, N. Wu, H.J. Li, W. L. Huang, Z.C. Ding, L.L. Gao, S.Z. Liu, K. Zhao, Amidino-based Dion-Jacobson 2D perovskite for efficient and stable 2D/3D heterostructure perovskite solar cells, Joule 7 (3) (2023) 574–586.

[42] M.H. Wang, Y.F. Yin, W.X. Cai, J. Liu, Y.L. Han, Y.L. Feng, Q.S. Dong, Y.D. Wang, J. M. Bian, Y.T. Shi, Synergetic Co-modulation of crystallization and Co-passivation of defects for FAPbI3 perovskite solar cells, Adv. Funct. Mater. 32 (6) (2022) 2108567.

[43] J.W. Lee, Z.H. Dai, T.H. Han, C. Choi, S.Y. Chang, S.J. Lee, N. De Marco, H.X. Zhao, P.Y. Sun, Y. Huang, Y. Yang, 2D perovskite stabilized phase-pure formamidinium perovskite solar cells, Nat. Commun. 9 (2018) 3021.

[44] J.P. Zhang, L.L. Chu, T.J. Liu, B.K. Tian, W.C. Chu, X.N. Sun, R.M. Nie, W. Zhang, Z. H. Zhang, X.M. Zhao, W.L. Guo, Engineering spacer conjugation for efficient and stable 2D/3D perovskite solar cells and modules, Angew. Chem. Int. Ed. 64 (1) (2025) e202413303.

[45] G.Y. Chen, Z.D. Guo, X.G. Gong, W.J. Yin, Kinetic pathway of γ-to-δ phase transition in $CsPbI_3$, Chem 8 (11) (2022) 3120–3129.

[46] T.Y. Zhang, M.I. Dar, G. Li, F. Xu, N.J. Guo, M. Grätzel, Y.X. Zhao, Bication lead iodide 2D perovskite component to stabilize inorganic α-$CsPbI_3$ perovskite phase for high-efficiency solar cells, Sci. Adv. 3 (9) (2017) e1700841.

[47] Z.Z. Li, X.L. Liu, J. Xu, S.J. Yang, H. Zhao, H. Huang, S.F. Liu, J.X. Yao, 2D-3D $Cs_2PbI_2Cl_2$-$CsPbI_{2.5}Br_{0.5}$ mixed-dimensional films for all-inorganic perovskite solar cells with enhanced efficiency and stability, J. Phys. Chem. Lett. 11 (10) (2020) 4138–4146.

[48] J. Xu, J. Cui, S.M. Yang, Z.K. Liu, X. Guo, Y.H. Che, D.F. Xu, W.J. Zhao, N.Y. Yuan, J.N. Ding, S.Z. Liu, Stable high-efficiency $CsPbI_2Br$ solar cells by designed passivation using multifunctional 2D perovskite, Adv. Funct. Mater. 32 (33) (2022) 2202829.

[49] Z.X. Huang, F.Y. Jiang, Z.N. Song, K. Dolia, T. Zhu, Y.F. Yan, D.S. Ginger, Local a-site phase segregation leads to Cs-rich regions showing accelerated photodegradation in mixed-cation perovskite semiconductor films, ACS Energy Lett. 9 (6) (2024) 3066–3073.

[50] H. Zhai, F.Y. Liao, Z. Song, B. Ou, D. Li, D.Y. Xie, H. Sun, L.B. Xu, C. Cui, Y.Y. Zhao, 2D PEA_2PbI_4-3D $MAPbI_3$ composite perovskite interfacial layer for highly efficient and stable mixed-ion perovskite solar cells, ACS Appl. Energy Mater. 4 (12) (2021) 13482–13491.

[51] Q. Yao, Q.F. Xue, Z.C. Li, K.C. Zhang, T. Zhang, N. Li, S.H. Yang, C.J. Brabec, H. L. Yip, Y. Cao, Graded 2D/3D perovskite heterostructure for efficient and operationally stable MA-free perovskite solar cells, Adv. Mater. 32 (26) (2020) 2000571.

[52] T. Zhou, Z.Y. Xu, R. Wang, X.Y. Dong, Q. Fu, Y.S. Liu, Crystal growth regulation of 2D/3D perovskite films for solar cells with both high efficiency and stability, Adv. Mater. 34 (17) (2022) 2200705.

[53] Q. Chen, M.E. Ma, W.L. Li, Y. Wang, Y. Gao, Y. Li, C. Liu, Improved efficiency and stability of perovskite solar cells through long-chain phenylammonium additives, ACS Appl. Mater. Inter. 17 (3) (2025) 5193–5201.

[54] Z.Q. Wan, Y.X. Wang, H. Lu, R.M. Wei, H.M. Yin, H.B. Zeng, M. Azam, J.S. Luo, C. Y. Jia, Incorporation of 2D pyreneammonium iodide for enhancing the efficiency and stability of perovskite solar cells, Chem. Sci. 15 (40) (2024) 16618–16626.

[55] G.Z. Liu, H.Y. Zheng, X.X. Xu, S.D. Xu, X.X. Zhang, X. Pan, S.Y. Dai, Introduction of hydrophobic ammonium salts with halogen functional groups for high-efficiency and stable 2D/3D perovskite solar cells, Adv. Funct. Mater. 29 (47) (2019) 1807565.

[56] Z.L. Song, J. Yang, X.Y. Dong, R. Wang, Y.X. Dong, D.X. Liu, Y.S. Liu, Inverted wide-bandgap 2D/3D perovskite solar cells with >22% efficiency and low voltage loss, Nano Lett. 23 (14) (2023) 6705–6712.

[57] T.T. Liu, J.H. Guo, D. Lu, Z.Y. Xu, Q. Fu, N. Zheng, Z.Q. Xie, X.J. Wan, X.D. Zhang, Y.S. Liu, Y.S. Chen, Spacer engineering using aromatic formamidinium in 2D/3D hybrid perovskites for highly efficient solar cells, ACS Nano 15 (4) (2021) 7811–7820.

[58] B.B. Yu, Z.H. Chen, Y.D. Zhu, Y.Y. Wang, B. Han, G.C. Chen, X.S. Zhang, Z. Du, Z. B. He, Heterogeneous 2D/3D tin-halides perovskite solar cells with certified conversion efficiency breaking 14%, Adv. Mater. 33 (36) (2021) 2102055.

[59] A. Purkayastha, A.T. Mallajosyula, Performance of 2D/3D mixed-dimension tin perovskite solar cells and their prospects under bifacial configuration, IEEE J. Photo 15 (1) (2025) 54–60.

[60] S. Sandhu, R. Singh, K. Yoo, M. Kumar, J.J. Lee, Effect of binary additives in mixed 2D/3D Sn-based perovskite solar cells, J. Power Sources 491 (2021) 229574.

[61] F.Q. Du, H. Gu, W.Y. Jiang, W.H. Yang, Y.X. Lin, W.J. Zhu, X. Qin, X.Q. Xie, L.J. Bu, X.L. Liu, S.C. Yang, C. Liang, Managing crystallization and phase distribution via 2D perovskite seed crystals for 2D-3D tin-based perovskite solar cells, Adv. Funct. Mater. 35 (3) (2025) 2413281.

[62] Z.Y. Kang, P. Feng, K. Wang, L. Zhang, R. Meng, Y.L. Chen, J.D. Wu, F. Yang, X. W. Zhang, T.X. Li, J.Z. Shang, Y. Tong, H.Q. Wang, Synchronous dimension-crystallization engineering enables highly efficient 2D/3D tin perovskite solar cells, Energy Environ. Sci. 18 (9) (2025) 4108–4119.

[63] B.H. Chang, L. Wang, H. Li, L. Pan, Y.T. Wu, Z. Liu, Y.N. Zhang, E.Y. Guo, L.W. Yin, Phase-pure 2D/3D tin-based perovskite films for solar cells, ACS Energy Lett. 9 (2) (2024) 363–372.

[64] G. Xing, C.B. Li, W.Y. Gao, J.X. Yang, X.J. Zhao, J.P. Wang, X.Q. Ran, L.F. Chao, H. Huang, Y.P. Zhou, Y.H. Chen, Z.B. Wu, C.X. Ran, W. Huang, Molecule anchoring strategy promotes vertically homogeneous crystallization and aligned interfaces for efficient Pb-Sn perovskite solar cells and tandem device, Adv. Mater. 36 (40) (2024) 2404185.

[65] J.X. Yang, Z.L. Wang, X.J. Zhao, W.Y. Gao, G. Xing, X.B. Wang, L.X. Wang, C.B. Li, Y.Y. Wang, Y.M. Ren, W.J. Liu, F. Yang, J.X. Sun, H. Dong, L.F. Chao, Y.P. Zhou, Y. H. Chen, Z.B. Wu, C.X. Ran, W. Huang, Guiding vertical growth and improving the buried interface of Pb-Sn perovskite films with 2D perovskite seeds for efficient narrow-bandgap perovskite solar cells and tandems, Energy Environ. Sci. 18 (6) (2025) 2883–2894.

[66] R.L. Milot, R.J. Sutton, G.E. Eperon, A.A. Haghighirad, J.M. Hardigree, L. Miranda, H.J. Snaith, M.B. Johnston, L.M. Herz, Charge-carrier dynamics in 2d hybrid metal-halide perovskites, Nano Lett. 16 (11) (2016) 7001–7007.

[67] L. Wang, B.H. Chang, H. Li, Y.T. Wu, L.Y. Zhang, L.W. Yin, Electron acceptor molecule doping induced π-π interaction to promote charge transport kinetics for efficient and stable 2D/3D perovskite solar cells, Angew. Chem. Int. Ed. 62 (26) (2023) e202304256.

[68] J.S. Sun, N. Chandrasekaran, C. Liu, A.D. Scully, W.P. Yin, C.K. Ng, J.J. Jasieniak, Enhancement of 3D/2D perovskite solar cells using an F4TCNQ molecular additive, ACS Appl. Energy Mater. 3 (9) (2020) 8205–8215.

[69] E. Jokar, C.H. Chien, A. Fathi, M. Rameez, Y.H. Chang, E.W.G. Diau, Slow surface passivation and crystal relaxation with additives to improve device performance

and durability for tin-based perovskite solar cells, Energy Environ. Sci. 11 (9) (2018) 2353–2362.
[70] H.Y. Zheng, S.Y. Dai, K.X. Zhou, G.Z. Liu, B. Zhang, A. Alsaedi, T. Hayat, X. Pan, New-type highly stable 2D/3D perovskite materials: the effect of introducing ammonium cation on performance of perovskite solar cells, Sci. Chin. Mater. 62 (4) (2019) 508–518.
[71] L. Iagher, L. Etgar, Effect of Cs on the stability and photovoltaic performance of 2D/3D perovskite-based solar cells, ACS Energy Lett. 3 (2) (2018) 366–372.
[72] S.L. Yue, G.B. Wu, X. Li, K. Li, G.S. Huang, Y. Tang, H.Q. Zhou, Research progress of quasi-two-dimensional perovskite solar cells, Chem. J. Chin. Univ. 42 (6) (2021) 1648–1671.
[73] J.M. Hoffman, J. Strzalka, N.C. Flanders, I. Hadar, S.A. Cuthriell, Q. Zhang, R. D. Schaller, W.R. Dichtel, L.X. Chen, M.G. Kanatzidis, In situ grazing-incidence wide-angle scattering reveals mechanisms for phase distribution and disorientation in 2D halide perovskite films, Adv. Mater. 32 (33) (2020) 2002812.
[74] S.H. Liu, X.Y. Wang, Y. Zhong, X. Luo, Y.K. Liu, B.L. Gao, L.C. Tan, Y.W. Chen, Controlled crystal orientation and reduced lattice distortion with a cystamine dihydrochloride spacer for efficient and stable 2D/3D perovskite solar cells, J. Mater. Chem. A 13 (10) (2025) 7554–7562.
[75] T. Ye, A. Bruno, G.F. Han, T.M. Koh, J. Li, N.F. Jamaludin, C. Soci, S.G. Mhaisalkar, W.L. Leong, Efficient and ambient-air-stable solar cell with highly oriented 2D@3D perovskites, Adv. Funct. Mater. 28 (30) (2018) 1801654.
[76] Z. Wang, Q. Wei, X.D. Liu, L. Liu, X.Y. Tang, J. Guo, S.Q. Ren, G.C. Xing, D. W. Zhao, Y.H. Zheng, Spacer cation tuning enables vertically oriented and graded quasi-2D perovskites for efficient solar cells, Adv. Funct. Mater. 31 (5) (2021) 2008404.
[77] Y.T. Wu, B.H. Chang, L. Wang, H. Li, L. Pan, Z. Liu, L.W. Yin, Intrinsic dipole arrangement to coordinate energy levels for efficient and stable perovskite solar cells, Adv. Mater. 35 (18) (2023) 2300174.
[78] N. Zhou, Y. Zhang, Z.J. Huang, Z.Y. Guo, C. Zhu, J.Y. He, Q. Chen, W.T. Sun, H. P. Zhou, Mobile media promotes orientation of 2D/3D hybrid lead halide perovskite for efficient solar cells, ACS Nano 15 (5) (2021) 8350–8362.
[79] F. Gao, H. Li, B.X. Jiao, L.G. Tan, C.T. Deng, X.J. Wang, C. Luo, C.L. Zhan, E. Debroye, Y.C. Peng, Y. Yang, C.Y. Yi, Q. Zhao, Perovskite facet heterojunction solar cells, Joule 9 (2) (2025) 101787.
[80] W. Li, M.U. Rothmann, Y. Zhu, W.J. Chen, C.Q. Yang, Y.B. Yuan, Y.Y. Choo, X. M. Wen, Y.B. Cheng, U. Bach, J. Etheridge, The critical role of composition-dependent intragrain planar defects in the performance of $MA_{1-x}FA_xPbI_3$ perovskite solar cells, Nat. Energy 6 (6) (2021) 624–632.
[81] Y. Yang, C. Liu, O.A. Syzgantseva, M.A. Syzgantseva, S. Ma, Y. Ding, M.L. Cai, X. P. Liu, S.Y. Dai, M.K. Nazeeruddin, Defect suppression in oriented 2D perovskite solar cells with efficiency over 18% via rerouting crystallization pathway, Adv. Energy Mater. 11 (1) (2021) 2002966.
[82] J. Chen, D. Lee, N.G. Park, Stabilizing the Ag electrode and reducing J-V hysteresis through suppression of iodide migration in perovskite solar cells, ACS Appl. Mater. Inter. 9 (41) (2017) 36338–36349.
[83] Y.Q. Hu, T. Qiu, F. Bai, W. Ruan, S.F. Zhang, Highly efficient and stable solar cells with 2D $MA_3B_2I_9$/3D $MAPbI_3$ heterostructured perovskites, Adv. Energy Mater. 8 (19) (2018) 1703620.
[84] X.J. Zhu, S.N. Zuo, Z. Yang, J.S. Feng, Z.Y. Wang, X.R. Zhang, S. Priya, S.F. Liu, D. Yang, In situ grain boundary modification via two-dimensional nanoplates to remarkably improve stability and efficiency of perovskite solar cells, ACS Appl. Mater. Inter. 10 (46) (2018) 39802–39808.
[85] C. Liu, Y. Yang, H. Chen, I. Spanopoulos, A.S.R. Bati, I.W. Gilley, J.H. Chen, A. Maxwell, B. Vishal, R.P. Reynolds, T.E. Wiggins, Z.W. Wang, C.Y. Huang, J. Fletcher, Y. Liu, L.X. Chen, S. De Wolf, B. Chen, D. Zheng, T.J. Marks, A. Facchetti, E.H. Sargent, M.G. Kanatzidis, Two-dimensional perovskitoids enhance stability in perovskite solar cells, Nature 633 (8029) (2024) 359–364.
[86] D.J. Yu, F. Cao, C.L. Su, G.C. Xing, Exploring, identifying, and removing the efficiency-limiting factor of mixed-dimensional 2D/3D perovskite solar cells, Acc. Chem. Res. 56 (8) (2023) 959–970.
[87] D.J. Yu, F. Cao, J.F. Liao, B.Z. Wang, C.L. Su, G.C. Xing, Direct observation of photoinduced carrier blocking in mixed-dimensional 2D/3D perovskites and the origin, Nat. Commun. 13 (1) (2022) 6229.
[88] C. Ortiz-Cervantes, P. Carmona-Monroy, D. Solis-Ibarra, Two-dimensional halide perovskites in solar cells: 2D or not 2D? Chemsuschem 12 (8) (2019) 1560–1575.
[89] W.H. Zhao, P.F. Guo, C. Liu, N. Jia, Z.Y. Fang, L.F. Ye, Q. Ye, Y.D. Xu, A.P. Glotov, A.A. Novikov, V.A. Vinokurov, D. Harvey, D. Shchukin, H.Q. Wang, Laser derived electron transport layers with embedded p-n heterointerfaces enabling planar perovskite solar cells with efficiency over 25, Adv. Mater. 35 (31) (2023) 2300403.
[90] W.H. Zhao, P.F. Guo, J.H. Wu, D.Y. Lin, N. Jia, Z.Y. Fang, C. Liu, Q. Ye, J.J. Zou, Y. Y. Zhou, H.Q. Wang, TiO_2 electron transport layer with p-n homojunctions for efficient and stable perovskite solar cells, NanoMicro Lett. 16 (1) (2024) 191.
[91] L.F. Ye, J.H. Wu, S. Catalán-Gómez, L. Yuan, R.M. Sun, R.H. Chen, Z. Liu, J. M. Ulloa, A. Hierro, P.F. Guo, Y.Y. Zhou, H.Q. Wang, Superoxide radical derived metal-free spiro-OMeTAD for highly stable perovskite solar cells, Nat. Commun. 15 (1) (2024) 7889.
[92] R. Wang, Y. Tong, A. Manzi, K. Wang, Z.D. Fu, E. Kentzinger, J. Feldmann, A. S. Urban, P. Müller-Buschbaum, H. Frielinghaus, Preferential orientation of crystals induced by incorporation of organic ligands in mixed-dimensional hybrid perovskite films, Adv. Opt. Mater. 6 (6) (2018) 1701311.
[93] A.A. Sutanto, R. Szostak, N. Drigo, V.I.E. Queloz, P.E. Marchezi, J.C. Germino, H.C. N. Tolentino, M.K. Nazeeruddin, A.F. Nogueira, G. Grancini, In situ analysis reveals the role of 2D perovskite in preventing thermal-induced degradation in 2D/3D perovskite interfaces, Nano Lett. 20 (5) (2020) 3992–3998.
[94] R. Zhi, C.Q. Yang, M.U. Rothmann, H.Q. Du, Y. Jiang, Y.Y. Xu, Z.W. Yin, Y.P. Mo, W. Dong, G.J. Liang, U. Bach, Y.B. Cheng, W. Li, Direct observation of intragrain defect elimination in $FAPbI_3$ perovskite solar Cells by two-dimensional PEA_2PbI_4, ACS Energy Lett. 8 (6) (2023) 2620–2629.